UNIVERSITY OF CALIFORNIA

Santa Barbara

Ductile-Phase-Toughened Tungsten for Plasma-Facing Materials

A Thesis submitted in partial satisfaction of the

requirements for the degree Master of Science

in Materials

by

Kevin Hawkins Cunningham

Committee in charge:

Professor G. Robert Odette, Chair

Professor Carlos G. Levi

Professor Francis W. Zok

December 2015

The thesis of Kevin Hawkins Cunningham is approved.

_____
Carlos G. Levi

_____
Francis W. Zok

_____
G. Robert Odette, Committee Chair

September 2015

Ductile-Phase-Toughened Tungsten for Plasma-Facing Materials

Kevin Hawkins Cunningham

ACKNOWLEDGEMENTS

This work was made possible by a number of talented and supportive people. I thank my advisor, Professor G. Robert Odette, for always encouraging me to learn more and push further, and for believing in my ability to do so. I also thank Professors Carlos Levi and Frank Zok for their guidance in academics and in this research. Our collaboration with Rick Kurtz and Chuck Henager provided valuable insights on the scope and direction of this project. The Odette research group has consistently supported me throughout my time here, and exchanging ideas on the group's various projects has given me a wider understanding of nuclear materials research. Special thanks go to David Gragg and Kirk Fields, whose engineering expertise continues to impress me, and who performed the mechanical testing described in this work. I thank Deryck Stave for his support in using various composite fabrication tools. I am grateful for assistance from the Materials Department staff and students throughout my studies. Finally, I thank my fiancé, my parents, and the rest of my family and friends for their personal support and encouragement in all aspects of my life.

ABSTRACT

Ductile-Phase-Toughened Tungsten for Plasma-Facing Materials

by

Kevin Hawkins Cunningham

A variety of processing approaches were employed to fabricate ductile-phase-toughened (DPT) tungsten (W) composites. Mechanical testing and analytical modeling were used to guide composite development. This work provides a basis for further development of W composites to be used in structural divertor components of future fusion reactors.

W wire was tested in tension, showing significant ductility and strength. Coatings of copper (Cu) or tungsten carbide (WC) were applied to the W wire via electrodeposition and carburization, respectively. Composites were fabricated using spark plasma sintering (SPS) to consolidate W powders together with each type of coated W wire. DPT behavior, e.g. crack arrest and crack bridging, was not observed in three-point bend testing of the sintered composites.

A laminate was fabricated by hot pressing W and Cu foils together with W wires, and subsequently tested in tension. This laminate was bonded via hot pressing to thick W plate as a reinforcing layer, and the composite was tested in three-point bending. Crack arrest was observed along with some fiber pullout, but significant transverse cracking in the W plate confounded further fracture toughness analysis.

The fracture toughness of thin W plate was measured in three-point bending. W plates were brazed with Cu foils to form a laminate. Crack arrest and crack bridging were observed in three-point bend tests of the laminate, and fracture resistance curves were successfully calculated for this DPT composite.

An analytical model of crack bridging was developed using the basis described by Chao in previous work by the group. The model uses the specimen geometry, matrix properties, and the stress-displacement function of a ductile reinforcement ("bridging law") to calculate the fracture resistance curve (R-curve) and load-displacement curve (P-D curve) for any test specimen geometry. The code was also implemented to estimate the bridging law of an arbitrary composite using R-curve data.

Finally, a parametric study was performed to quantitatively determine the necessary mechanical properties of useful toughening reinforcements for a DPT W composite. The analytical model has a broad applicability for any DPT material.

TABLE OF CONTENTS

LIST OF FIGURES

LIST OF TABLES

NOMENCLATURE

Bridging law	The stress-displacement function of a composite reinforcement material
Case 1	An implementation of the large-scale crack bridging model that calculates the R-curve and P-D curve of a composite test specimen from specimen geometry and material properties including the bridging law.
Case 2	A code implementation that estimates the parameters of the bridging law from specimen geometry, material properties, and R-curve test data.
DBTT	Ductile-brittle transition temperature
DPT	Ductile phase toughening; ductile-phase-toughened
Edge & face	Orientations of brazed laminate specimens, indicating crack propagation parallel (edge) or perpendicular (face) to the laminate layers.
L & T	Orientations of rolled W plate and laminate specimens, indicating crack propagation parallel (L) or perpendicular (T) to the rolling direction.
P-D curve	Plot of load vs. crosshead displacement
PFC	Plasma-facing component of a nuclear fusion reactor
PFCM	Plasma-facing component material
R-curve	Plot of fracture resistance vs. crack length
SPS	Spark plasma sintering; spark-plasma-sintered
SPD	Severe plastic deformation

NOMENCLATURE (CONT.)

K_{IC}	Fracture toughness of brittle matrix
$K_{I,P}$	Mode I stress intensity at the crack tip due to the applied load
$K_{I,F}$	Mode I stress intensity at the crack tip due to a pair of point forces on the crack face
$K_{IR}(da)$	Fracture resistance curve
$\Delta_P(x)$	Crack opening displacement distribution due to remote loading
$\Delta_F(x)$	Crack closing displacement distribution due to bridging tractions
$\Delta(x)$	Net crack-face displacement distribution; crack shape
$\sigma(x)$	Bridging stress distribution
$\sigma(\Delta)$	Bridging law
σ_{max}	Maximum stress in the bridging law
Δ_1	Displacement at maximum stress in the bridging law
n	Post-peak shape parameter in bridging law
Δ_2	Failure displacement of reinforcement
P' & D'	Failure load and displacement of a pure W test specimen with equivalent geometry for comparison to laminate data
D_F	Reduction in load-point displacement due to the bridging zone
R^2	Goodness-of-fit value for linear regression
s, w, a	Span, width, and crack length of specimen
a_0	Precrack length
c	End of bridging zone
F_1, F_2, V_2	Dimensionless functions of a/w specific to a given specimen geometry
E'	Plane strain elastic modulus
ν	Poisson's ratio
G	Shear modulus

1. Introduction

The objective of this study is to develop the materials science of tungsten (W) composites as candidates for plasma-facing components (PFCs) in future fusion reactors [1-6]. Tungsten and W-alloys are the leading candidates for the PFCs of future fusion reactors, such as the International Thermonuclear Experimental Reactor (ITER) and Demonstration Power Plant (DEMO), because of their high melting point, strength at high temperatures, and low sputtering yield [7-11]. In the design for ITER, W is implemented solely as a non-structural armor in the divertor component. An excellent overview of the divertor design may be found in recent work by Merola et al. [12] The goal for this study and others worldwide is to develop structural W materials to enable advanced divertor designs [13].

Tungsten and most W alloys exhibit low fracture toughness (K_{IC}) and a high ductile-brittle transition temperature (DBTT) that would render them as brittle materials in pulsed reactor operations [7, 9, 14]. The DBTT for unirradiated W-alloys typically ranges from 573K to 1273K (300 to 1000°C) and in a reactor environment radiation hardening would further elevate this range [9, 15, 16]. Metallurgical approaches to toughen W alloys, including alloying with rhenium (Re) and severe plastic deformation (SPD), have resulted in modest DBTT decreases [15, 17]. However, they would be difficult or impossible to implement, due to high costs and implications to irradiation hardening (W-Re alloys) or complex processing demands (SPD) [18-20]. To prevent mechanical failure, a toughening mechanism is needed for W before it can be considered an effective plasma facing component material (PFCM).

There are several types of tungsten under consideration for fusion reactor components. These include the oxide dispersion strengthened alloy WL10 (W-1.0La_2O_3),

the cemented composite MT-185 (W-2.1Ni-0.9Fe), and other fiber-reinforced or laminated composites with a variety of secondary/debonding phases [13, 21]. Composite development is still in the early stages, and these materials are not available on a commercial scale.

W-alloys toughened by engineered reinforcement architectures, such as ductile-phase toughening (DPT), are strong candidates for PFCMs. Previous work on a commercial W-Cu material was promising, showing nearly a threefold improvement in fracture resistance over monolithic W by reinforcing the matrix with 50% Cu by volume [2]. Copper is not a viable reinforcement choice for DPT tungsten PFCMs because of its relatively low melting point; however, it is useful for fabricating model composites because it is immiscible in W [22].

This study aims to demonstrate DPT in a model W composite, and to preserve and advance the analytical modeling of DPT materials. This thesis will first describe the experimental methodology and results of fabricating and testing W composites, followed by the approach and results of computational efforts.

2. Experimental Procedures

2.1 Ductile Phase Toughening

In DPT, a ductile phase is included in a brittle matrix to prevent fracture propagation. This is accomplished by the formation of an intact bridging zone behind the crack tip, which provides reinforcement, resulting in an increase in the remote load stress intensity for continued crack growth with increasing crack length [23-25]. The principles of DPT are illustrated in Figure 2.1, which shows ductile bridging ligaments stretching across an open crack in a W-Cu composite [3].

For a brittle material containing a suitable volume fraction of a ductile phase, a highly effective resistance curve toughening mechanism develops as the crack extends. As the crack propagates through a brittle matrix, it leaves a bridging zone of ductile ligaments over a length L behind the crack tip. As the crack extends, L increases. The ligaments act in opposition to the applied loading stress intensity factor, $K_{I,P}$. This reduces the effective crack tip stress intensity factor so that $K_{I,eff} < K_{I,P}$. For small-scale bridging, when the bridging zone is much smaller than the length of the crack, the bridging zone size and the fracture resistance both reach steady-state values. This study focuses on large-scale bridging, where the material fracture resistance does not reach a steady-state value for a small test specimen. The crack opening (Δ) increases with increasing distance behind the crack-tip until the reinforcement breaks at its failure displacement, Δ_2 [23-25].

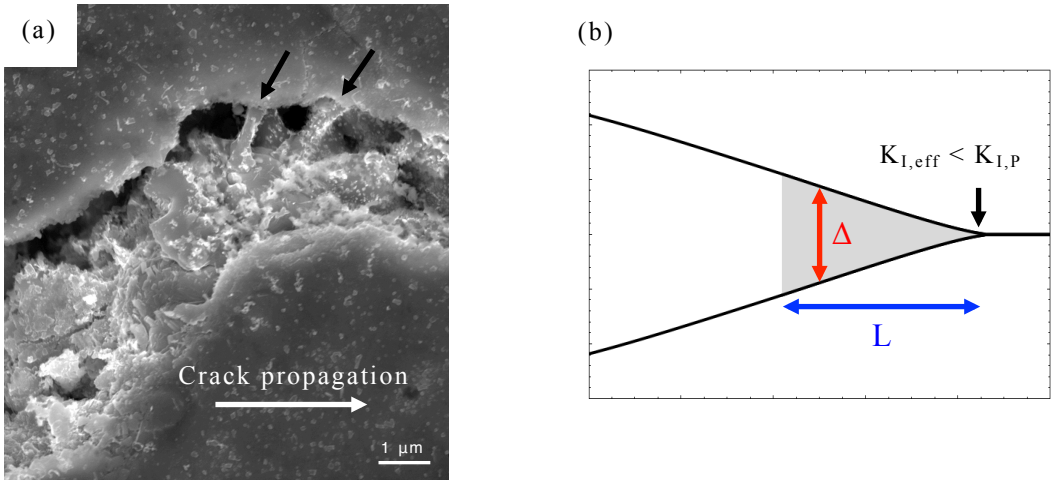

Figure 2.1. a) SEM image of Cu ligaments (indicated by black arrows) bridging a crack in a W-Cu composite. b) Schematic of cracked material oriented showing crack-face displacement (Δ) and bridging zone length (L). The effective stress intensity at the crack tip is shielded by a reinforcing material (the shaded area) [3].

There are many choices for ductile phases. Copper is useful for fabricating model W composites because it is immiscible with W and does not form brittle intermetallic phases [22]. Another option explored in this study is W wire, which has high strength and some

ductility, and can be coated with a weak debonding interface material. Maximizing the volume fraction of W in the final composite is preferable for reducing activation and plasma contamination in a fusion reactor [26], so W wires are an attractive reinforcement option.

2.2 Materials

Elemental W powder of 99.95% purity with a particle size of 4-6μm from Stanford Materials was used in this study. An additional W powder, cryogenically milled from this pure 4-6μm precursor at Aegis Technology, was also examined, but ultimately not used because it contained tantalum oxide impurities. The pure powders were consolidated via spark plasma sintering (SPS) to form pure W disks and composites.

Tungsten wires of varying diameter (15, 250, and 500 μm, 99.95% purity) were ordered from Alfa Aesar for use as ductile reinforcements. Each wire size was tested in tension, and 250-μm wire was used in fabricating both sintered and hot-pressed composites.

Tungsten and copper foils were ordered from ESPI Metals (W, 99.98% purity) and Basic Copper (Cu, 99.9% purity), respectively, with nominal thickness 127 μm. Both materials were tested in tension and then used to fabricate a hot-pressed laminate.

Tungsten plate of 1 ± 0.2 mm thickness and 99.97% purity was ordered from Plansee, and subsequently sent to Production Lapping for lapping to smooth and parallel the top and bottom surfaces. Surface roughness after lapping was measured to be less than 1 μm. The material toughness was measured in precracked three-point bending and the plates were used to fabricate a brazed composite.

2.3 Fabrication Techniques

2.3.1 Spark Plasma Sintering

Disk-shaped specimens were consolidated from elemental W powders using spark plasma sintering. SPS is a rapid consolidation technique that uses an electric current to heat a conductive powder directly (insulating powders are heated by the conductive die set) combined with uniaxial compression in a vacuum chamber. Figure 2.2 shows a schematic diagram of the SPS process.

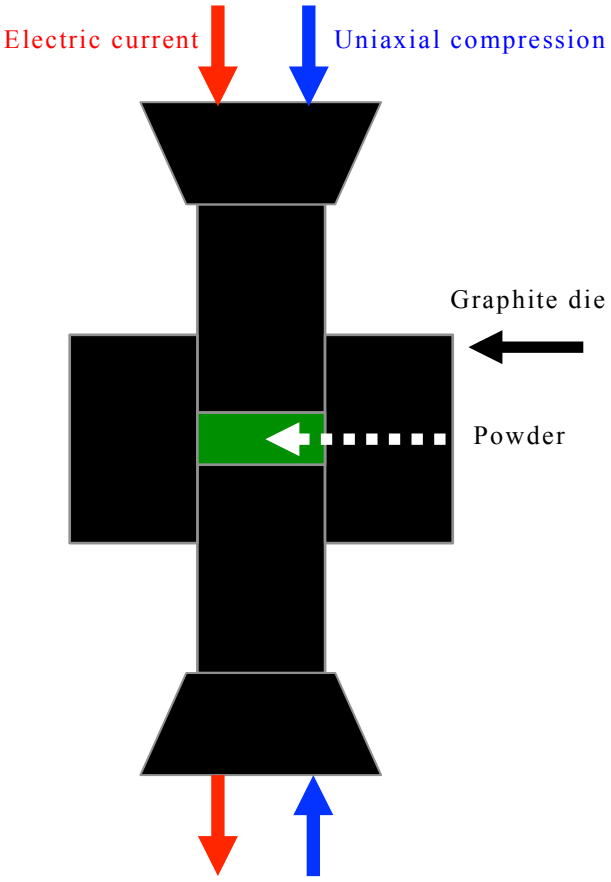

Figure 2.2. Schematic diagram of SPS process. An electric current heats the die set and powders. The powder is loaded in uniaxial compression.

The powder was loaded under an argon environment into a 20-mm inner-diameter graphite die with a layer of 0.15” graphite foil between the powder and die. Additional

specimens were prepared using 0.005” niobium (Nb) foil instead of graphite foil, to reduce formation of tungsten carbide [27]. When using Nb foil, one layer of foil was used for each face of the disk, and two layers were used around the circumference of the die. An initial study of the effect of temperature and dwell time on density was carried out to optimize the process. Composites were fabricated by laying up coated W wires within the W powder in the SPS die and consolidating the mixture.

Sintering temperatures between 990 and 1900 °C were used for various specimens as detailed later in this report. Dwell times up to 1 hour were used. The heating rate was 100 °C/min for each specimen, and continuous electric current was used (in contrast to a pulsed current).

After sintering, the disks were polished to remove any residual graphite. The disks were sectioned using a low-speed diamond saw (Buehler), then mounted and polished to 0.5 μm. A 5 x 5 mm section was also cut for density measurements. The grain size was determined optically after etching in a 30% hydrogen peroxide solution for 10 minutes in an ultrasonic bath [28].

2.3.2 Electrolytic Plating

Copper is a good choice for fabricating model W composites because of its immiscibility in W. Plating W wires with Cu was investigated as a means of creating a weak debond layer for the composite. To prepare the wires for plating, first they were wiped with mineral oil to remove large particles, then soaked in an ultrasonic bath at 50°C for 15 minutes (solution: 0.1g sodium carbonate, 0.3g sodium borate in 19.6g water). The clean wires were plated at 50°C under direct current, 162 A per m^2 of immersed wire (aqueous solution of 0.625M sulfuric acid, 0.4M copper sulfate, and 2 g/L urea) [29-31].

A small-scale plating apparatus was constructed using a rectangular bath (3 x 5 cm by 10 cm tall) with three bus wires running above the plating solution. The two outer bus wires were connected and Cu wire was hung from them to form the cathode. W wire was hung from the center bus to form the anode (See Fig. 2.3 for diagram). Eight lengths of tungsten wire were plated simultaneously for 35 minutes with approximately 8cm immersed in the plating solution for each. Plating thickness was measured with a micrometer.

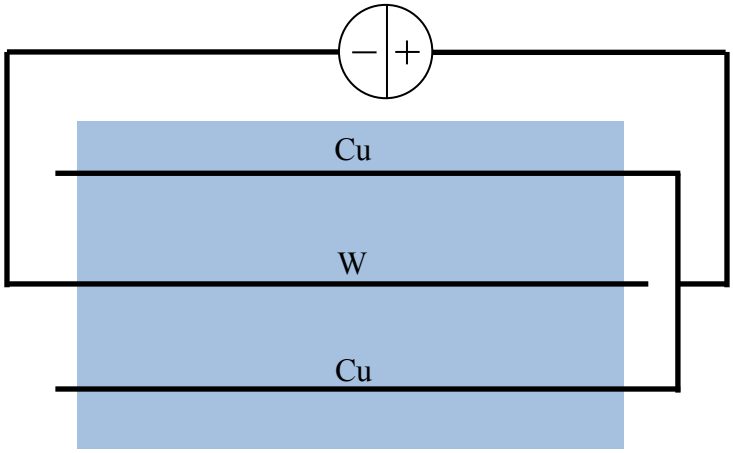

Figure 2.3. Top-down schematic of plating apparatus. The bare wire above the plating bath allows multiple lengths of current-carrying wire to be suspended within the bath. The W and Cu labels indicate the wire that hangs from each bus [2].

2.3.3 Carburization

Tungsten carbide was investigated as a potential highly stable debonding layer because C is a suitable element for the divertor in terms of low neutron activation and reduced potential for plasma contamination [26]. 12-mm lengths of 250-μm W wire were placed apart in loose graphite powder (2-15 μm particle size, Alfa Aesar), and then compacted at 35 MPa at ambient temperature in the SPS system. The compact was heat treated at 1800°C for 1 minute under vacuum with a heating ramp of 300°C/min under a minimum load of 9 MPa. Coated wires were cleaned in an ultrasonic bath to remove excess graphite particles.

2.3.4 Hot Pressing

To avoid the issue of Cu melting and wicking during the sintering of a W matrix, a hot-pressing fabrication route was developed for W wires sandwiched between W and Cu foils, as illustrated in Figure 2.4a-b. The top and bottom layers were 127-µm W foils. The inner layers were the 127-µm Cu foils, while the middle layer contained 250-µm W wires. The laminate was 50 x 50mm, with an average of 50 µm at the shortest distance between the parallel fibers. After hot pressing at 900°C at 38 MPa for 5 minutes, the W-wires were embedded in the Cu, forming a 3-layer sandwich.

The W-foil / Cu / W-wire sandwich reinforcement was then hot pressed between 4-mm thick W plates, as illustrated in Figure 2.4c. Since the surface roughness of the reinforcement was ≈ 100 µm, reflecting the underlying topology of the stronger W-wires, a Cu bond layer of 127-µm foil was used between the W-plates and sandwich. The volume fraction of Cu was approximately 10% in the laminate as shown in Figure 2.4c.

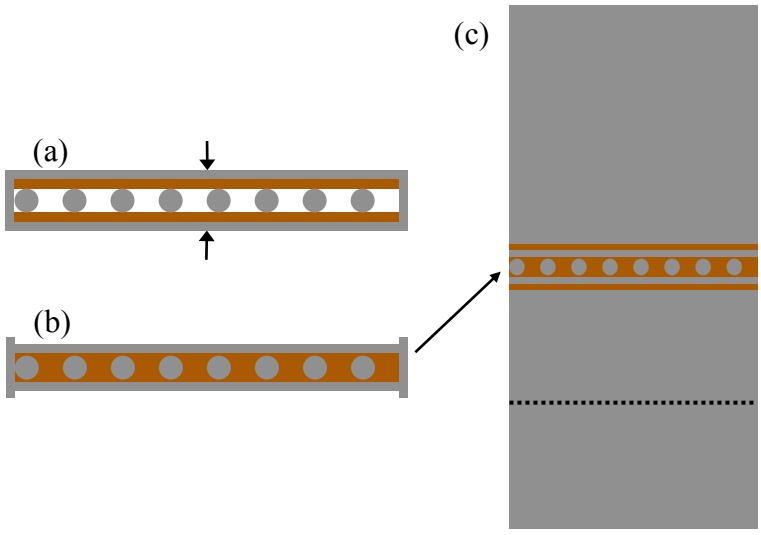

Figure 2.4. Schematic diagram of hot-pressed reinforcement cross-section a) before and b) after hot pressing, as well as c) the schematic diagram of hot-pressed bend specimen cross-section. Dashed line indicates notch depth. Note that images (a) and (b) are the same scale, while (c) is not [4].

2.3.5 Brazing

Diffusion bonding of W to Cu via hot pressing was found to be inconsistent, so brazing W plates with thin layers of Cu was explored. Lapped 0.85 x 50 x 50 mm W plates were stacked alternating with 75-μm Cu foils, and secured with stainless steel wire. The W plates were aligned using the rolling direction. One of the outer plates was rotated 90° from the others, as will be discussed later. The layup was heated in an Ar-5%H_2 environment to 1113 °C at 15 °C/min and held for 6 s before cooling.

2.4 Measurements and Mechanical Tests

2.4.1 Microhardness Testing

The hardness of the SPS-consolidated W was measured using a Leco M-400A microhardness tester. A series of 8-10 indents was made along the cross-section of each disk with a load of 500g. Indent locations were chosen manually to avoid scratched areas. The hardness of the W wire was measured before and after several high-temperature processing steps using the same methods.

2.4.2 Density Measurements

The density of SPS-consolidated disks was calculated using a Micrometrics AccuPyc 1330 helium pycnometer. Disk sections were cleaned, dried, and weighed on a balance to an accuracy of 10 μg. For each pycnometer measurement, the instrument was calibrated with a reference volume and the sample volume was taken as the average of 10 measurements.

2.4.3 Tensile Testing

Tensile testing of 15-, 250-, and 500-μm tungsten wire was performed using techniques and equipment developed for ceramic fiber testing. The 15-μm wire specimens

were prepared by mounting each length of wire to a rigid holder with epoxy, and then severing the holder once installed in the grips. The 250- and 500-μm wire specimens were prepared by sandwiching the ends of each wire section in epoxy between two polyamide plates. Tests were performed at ambient temperature in air at a crosshead displacement rate of 0.5 mm/min.

Tensile tests were performed on 127 μm thick W and Cu foils at a strain rate of 0.011 min^{-1} at ambient temperature in air, with a gauge length and width of 9 mm and 2 mm, respectively. Specimens were prepared by punching directly from the stock material. Strain was measured with a laser extensometer.

Tensile test samples of the hot-pressed W-Cu reinforcement (See Fig. 2.4b) were EDM-cut with a gauge length, width, and thickness of 6.4 mm, 2.45 mm, and 0.8 mm, respectively. The tensile direction was parallel to the wire direction. Tensile testing was performed with crosshead displacement rates of 0.1 and 0.1125 mm/min at ambient temperature in air.

2.4.4 Fracture Testing

Notched specimens of the W-WC sintered composite were tested in three-point bending with the goal of observing debonding behavior during crack propagation. Notched three-point bend test samples were EDM-cut with a test span, width, thickness, and notch depth of 10 mm, 3.6 mm, 3.6 mm, and 0.5 mm, respectively. The crack propagation direction was perpendicular to the wire direction. Bend testing was performed with a crosshead displacement rate of 0.05 mm/min at ambient temperature in air.

For the hot-pressed W-Cu composite, notched three-point bend test samples were EDM cut with a test span, width, thickness, and notch depth of 27.6 mm, 8.9 mm, 3.1 mm,

and 2 mm, respectively. The crack propagation direction was perpendicular to the wire direction. Bend testing was performed with a crosshead displacement rate of 0.02 mm/min at ambient temperature in air.

For the 1-mm W plates, notched bend bars were EDM-cut with dimensions 21 x 4.65 x 0.85 mm with a notch depth of 0.93 mm. Specimens were pre-cracked by standing them upright in a load frame with the span along the fatigue loading direction as shown in Figure 2.5. The specimens were compression-compression fatigued at 20 Hz and the crack length was observed at intervals of 10,000 cycles until reaching a length of approximately a/w = 0.3. The pre-crack depth was marked by applying a dye penetrant prior to fracture testing and observed on the fracture surface. Tests were performed on a 20.5-mm span at ambient temperature in air with a crosshead displacement rate of 0.05 mm/min.

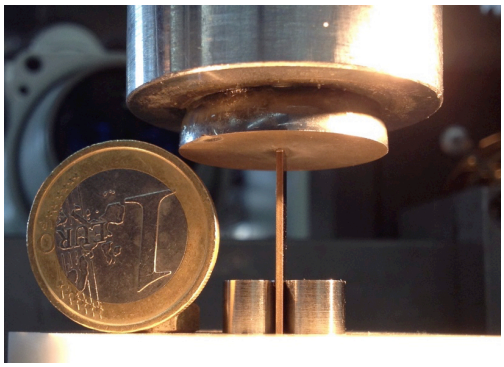

Figure 2.5. Photograph of end-on compression fatigue setup for 0.85-mm thickness W bend bars. A steel clip is used to help stand the specimen upright. A coin is shown for scale [5].

For the W-Cu brazed laminate, notched three-point bend bars were EDM-cut with dimensions 21 x 4.65 x 2.125 mm with a notch depth of 0.93 mm. Specimens were separated into “edge” and “face” categories, for which the direction of crack propagation was normal to the edge or face of the ductile laminate layers, respectively. Specimens were labeled “L” or “T” with respect to the rolling direction of the W plates they contained, indicating if the crack propagation direction was parallel (L) or perpendicular (T) to the

rolling direction. Additional specimens were created with a mixture of L and T plates, called L+T.

Several specimens were fatigued in three-point bending to attempt to develop a precrack, without success. Those that did not develop a pop-in to a/w≈0.9 were tested on a 20.5-mm span at a crosshead displacement rate of 0.1 mm/min.

The majority of brazed laminate specimens were pre-cracked to a/w≈0.3 in compression-compression fatigue, similar to the pure W plate specimens. Tests were performed on a 20.5-mm span at ambient temperature in air at a crosshead displacement rate of 0.05 mm/min. A microscope mounted on the load frame was used to observe the increments of crack growth for correlation with the load-displacement data. The crack shape at the end of each test was marked by oxidizing the W surface at 400°C in air.

2.5 Data Analysis

2.5.1 Tensile Testing

Engineering stress was calculated using the initial cross-section of the test specimen. For the W wires, the yield stress was calculated using an analogy to the 0.2% strain offset method, where the displacement divided by the initial gauge length was used instead of strain. For the pure W and Cu foils, yield stress was calculated using the 0.2% strain offset method. For the hot-pressed laminate reinforcement, engineering stress was calculated using the initial cross-section of all material in the laminate, excluding porosity, for the initial elastic loading. After the load drop, engineering stress was calculated assuming only the Cu foils were intact.

2.5.2 Fracture Testing

For three-point bend tests, the maximum load at each increment of measured crack length was used to calculate the fracture resistance corresponding to the arrested crack length following ASTM E399-12 [32]. For toughness measurements of brittle materials such as the W plate, only the initial precrack length was used. For the W-Cu brazed laminate, multiple crack lengths were measured during each test, giving rise to a resistance [K_{IR}(da)] curve associated with crack bridging by the ductile layer.

Some composite test specimens were not precracked, and as such they cannot provide real fracture toughness data. Nevertheless, these tests still guided fabrication efforts by indicating whether debonding occurred between the matrix and reinforcement.

3. Experimental Results

3.1 Materials

3.1.1 Tungsten Wire

Table 3.1 summarizes the tensile properties of W-wire of various diameters. A general trend of increased strength and decreased ductility is observed as the wire diameter decreases. The tested specimens were examined microscopically to verify cup-and-cone fracture to confirm uniform stress distribution in the wire. The ultimate strength reached a remarkable value of 4.31 GPa in the 15-μm wire, with about 1.0% total elongation. The larger diameter wires had lower strength but showed greater total elongation.

Table 3.1. Average values of W wire properties from tensile testing [4].

Diameter (µm)	Yield Stress (MPa)	Ultimate Tensile Strength (MPa)	Total Elongation (%)	Reduction in Area (%)
15	3.58	4.31	1.0	N/A
250	1.78	2.31	1.7	29.9
500	1.34	2.12	2.4	27.1

The 250-µm W wires, used to make various composites, were analyzed with EBSD to quantify how their properties evolved after several of the high-temperature fabrication steps. After processing at 1900°C for 5 minutes during the carburization process described above, a decrease in texture strength and a higher fraction of smaller grains was observed in the W wire as shown in Figure 3.1.

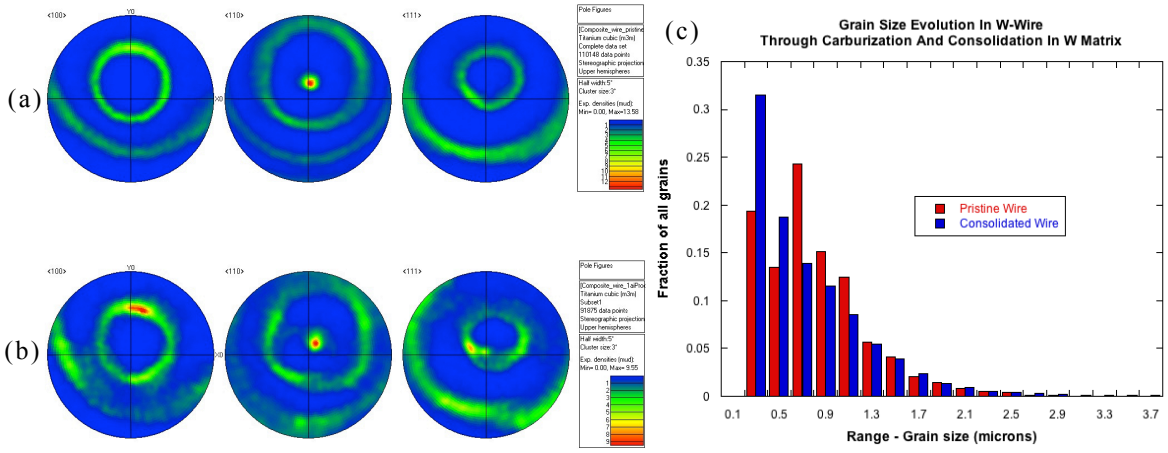

Figure 3.1. Microstructure evolution in W wire during processing to form W-WC composite. a) Pole figure contour maps for pristine wire showing {110} texture out of plane (axial direction of the wire). b) Pole figure contour maps for W wire after consolidation in composite showing qualitatively weaker {110} texture out of plane (more diffuse peaks). c) Histogram of grain sizes shows a higher fraction of smaller grains after processing. Note that in parts (a) and (b), the difference in the scan areas (110148 and 91875 data points, respectively) convolutes a quantitative interpretation of the difference in the peak intensities (13.58 and 9.55, respectively), requiring instead a qualitative comparison of peak sharpness.

The hardness of the wire decreased about 9% (from 673.6 to 613.0 HV) after 370 minutes at 900°C through 3 processing steps: 1) hot pressing at 38 MPa in vacuum for 5 minutes, 2) an oxide reduction in Ar-5%H_2 for 360 minutes, and 3) hot pressing at 34 MPa in vacuum for 5 minutes.

3.1.2 Tungsten and Copper Foils

Representative stress-strain curves for the pure tungsten and copper foils are shown in Figure 3.2. The tensile properties are summarized in Table 3.2. The W-foil has a high strength and limited ductility. The Cu-foil has low strength, but high ductility.

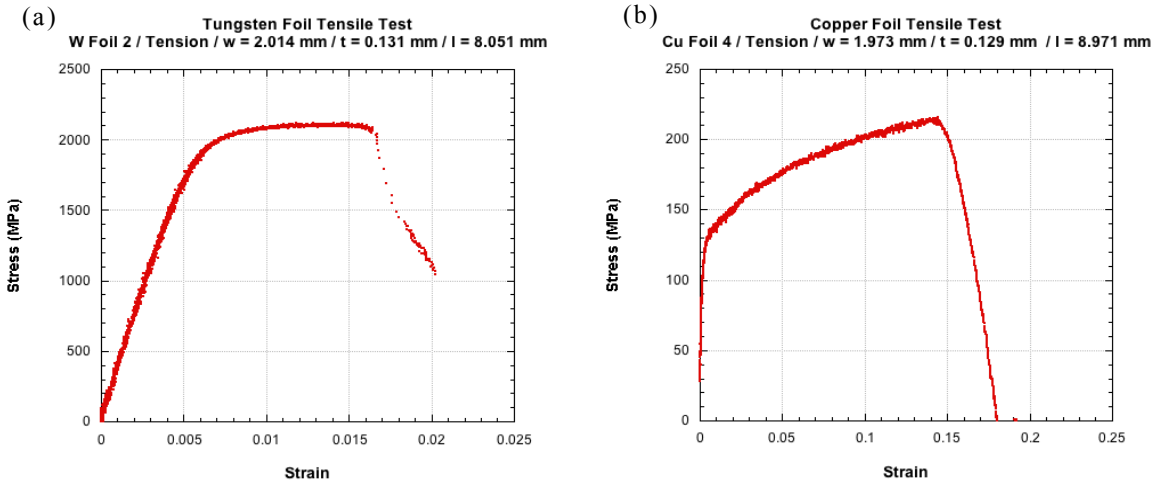

Figure 3.2. Representative stress-strain curves for a) tungsten and b) copper foils. Note the order-of magnitude differences for both the stress and strain axes between graphs [4].

Table 3.2. Summary of tensile data for W and Cu foils [4].

Material	Yield Stress (MPa)	Ultimate Tensile Strength (MPa)	Total Elongation (%)
W	1997.7 ± 10.5	2119.4 ± 4.5	3.4 ± 1.3
Cu	130.2 ± 4.6	218.7 ± 4.9	16.9 ± 3.3

3.1.3 Tungsten Plate

A summary of fracture toughness testing of the W plate in both the L and T orientations is shown in Table 3.3. The average W toughness and standard deviations were 13.06 ± 2.34 and 20.90 ± 0.45 MPa $m^{0.5}$ in the L and T directions, respectively.

Table 3.3. Summary of fracture toughness tests for pure W plate [5].

Specimen	a/w	Load (N)	Toughness (MPa $m^{0.5}$)
L2	0.26	101.60	10.5
L5	0.28	98.96	10.7
L6	0.33	120.70	14.7
L7	0.27	129.73	13.6
L8	0.31	135.54	15.7
T2	0.27	195.29	20.5
T3	0.30	190.81	21.5
T6	0.27	199.55	20.9
T8	0.26	200.55	20.8

3.2 Sintered Composites

The results of the SPS consolidation study for pure W powders are summarized in Table 3.4. These results were used to establish acceptable parameters for consolidating sintered composites.

Table 3.4. Summary of SPS conditions and W disk properties.

Temperature (°C)	Dwell Time (mins)	Density (% Max)	Hardness (HV)	Grain Size (μm)
1700	1	79.8	165.1 ± 6.1	6.1 ± 1.5
1700	60	92.0	332.4 ± 9.6	8.7 ± 3.0
1900	21	91.3	322.0 ± 9.2	9.0 ± 2.8
1900	60	92.1	338.6 ± 7.3	13 ± 5.8
1900*	60	93.9	343.6 ± 6.8	29 ± 6.5
1900*	5	95.2	224.6 ± 3.3	7.2 ± 3.8

The percent given for density references a maximum density of 19.3 g/cm^3 for pure single-crystal tungsten. In each case the heating rate was 100 °C/min approaching the maximum temperature and the uniaxial pressure was 50 MPa. Asterisks indicate samples prepared using Nb foil instead of graphite [2].

After electroplating, micrometer measurements indicated an average Cu coating thickness of 30 μm on the W wires. The carburization process resulted in a 12-μm layer of WC on the wire. The summary of SPS composite fabrication processes and outcomes is shown in Table 3.5.

Table 3.5. Summary of process parameters for SPS system and outcomes for composite fabrication and W-wire carburization. Multiple lines per row indicate sequential processes on the same material [3].

Materials	Pressing (MPa)	Heating rate (°C/min)	Dwell T (°C)	Dwell t (min)	Result
Cu-coated W wire + W	50	100	1700	5	Cu melted, found in matrix pores
Cu-coated W wire + W	50 50	100 100	990 1700	25 0	Cu melted, found in matrix pores
W wire + C	35 9.5	- 300	- 1800	- 1	12- μm WC coating on W wires
WC-coated W wire + W	50	100	1900	10	WC intact at interface

In the case of the Cu-coated wires, neither direct sintering nor an attempt to partially consolidate W at low temperature before finishing at high temperature was successful in maintaining a Cu layer at the wire-matrix interface. Instead, a small amount of wicked Cu was found via energy dispersive x-ray spectroscopy (EDS) to coat the porous matrix, as shown in Figure 3.3. In contrast, the 12-μm WC coating was intact after consolidation.

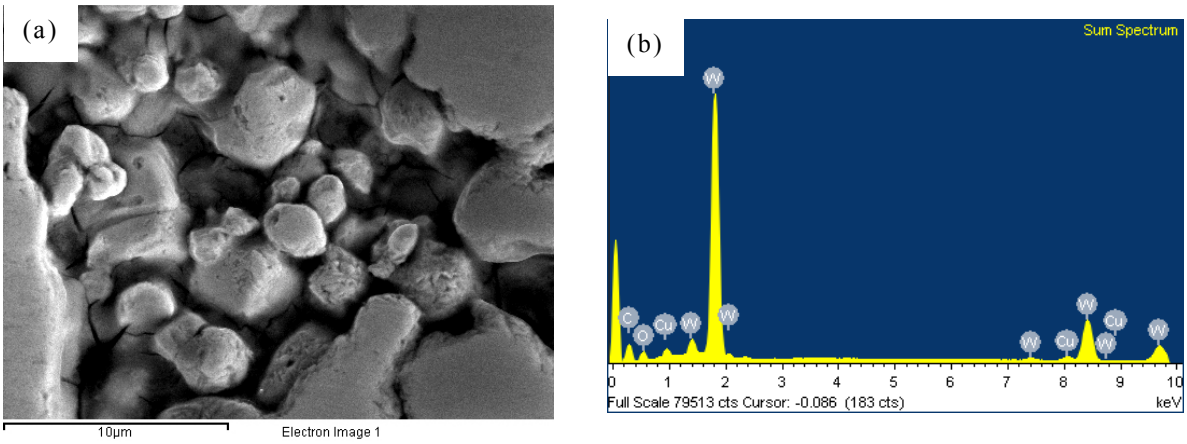

Figure 3.3. a) SEM image of a porous area in W matrix. Sample is single-temperature SPS route for W powder consolidated around Cu-coated W wires. b) EDS spectrum shows Cu detected in pore. The wire-matrix interface was characterized only by a change in porosity between the dense wire and the slightly porous matrix, and showed no contrast in scattering, microstructure, or chemistry (via EDS) [3].

No bridging was observed in the W-WC sintered composite, since the cracks ran directly though the coated wire without any debonding as shown in Figure 3.4. Despite the presence of some porosity at the WC-matrix interface, this may be due to the fact that the

WC layer was strongly bonded to both the W matrix and wire. Further analysis of chemistry and crystal structure may indicate the extent of reaction to form both WC and W_2C, and may help to explore the shift in fracture character in the wire from the edges to the center.

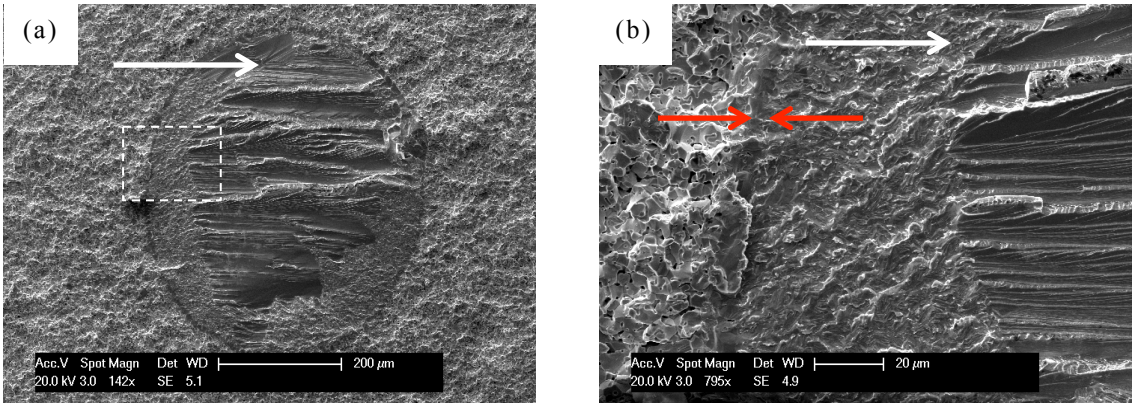

Figure 3.4. SEM images at 2 different magnifications of a W-WC bend bar fracture surface. White arrows indicate the direction of crack propagation. Red arrows show thickness of WC layer. There is no evidence of debonding along the W-WC interface.

3.3 Hot-Pressed Composites

The results of laminate reinforcement tensile testing are summarized in Figure 3.5. Note that the plot shows a single curve with a discontinuity, as the test was paused and resumed after the W foils cracked. The reinforcement showed some evidence of fiber pullout but no indication of plasticity in the W-wires. The outer W-foils cracked at the peak stress, followed by fracture of the W-wires. Deformation occurred in the Cu layer at a much lower stress until ductile failure.

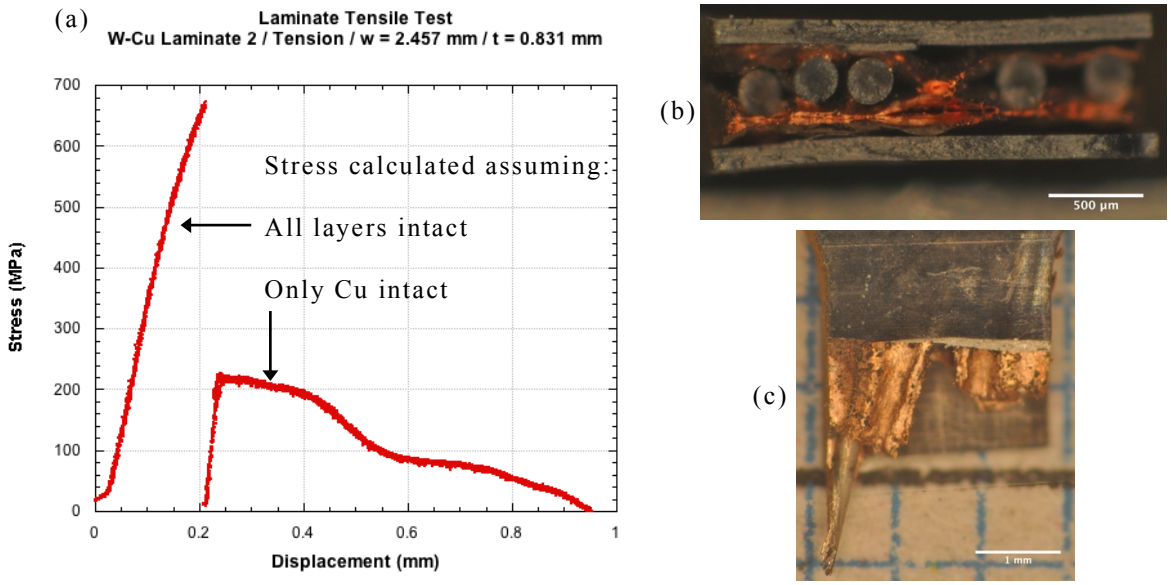

Figure 3.5. Summary of laminate reinforcement tensile tests. a) The stress-displacement curve uses the initial cross-sectional area of entire specimen for elastic loading, and the cross-sectional area of Cu only for plastic region. b) Fracture surface of specimen 1. Necking is seen in Cu but not in W foil or wire. c) Protruding W wire from specimen 2 suggests energy dissipation by pullout [4].

The results of laminate fracture testing are summarized in Figure 3.6. The stress was calculated using the applied load and initial geometry of the test specimen. In one test (specimen 1), the crack propagated through the W plate up to the embedded laminate and re-nucleated on the other side, leaving the reinforcement sandwich intact. At this point the specimen could only sustain a low load of ≈ 130 N. In a second test (specimen 2), cracks grew from the notch parallel to the sandwich, before branching with one crack deflecting 90° and propagating up to the sandwich at the first pop-in stress drop. This crack arrested and the stress increases again until the crack re-nucleated at the back of the sandwich marked by the second stress drop. However, the laminate composite was still able to sustain a significant load in this case, which actually then increased prior to a gradual drop-off associated with continued deformation of the sandwich layer. Removing the Cu using a nitric acid bath showed that several of the W wires had fractured between 0.075 to 1.4 mm

away from the bending point, indicating that fiber pullout could play a role in the mechanical response of the composite. Peak-load stress intensity factor values ranged from 20 to 34 MPa $m^{0.5}$.

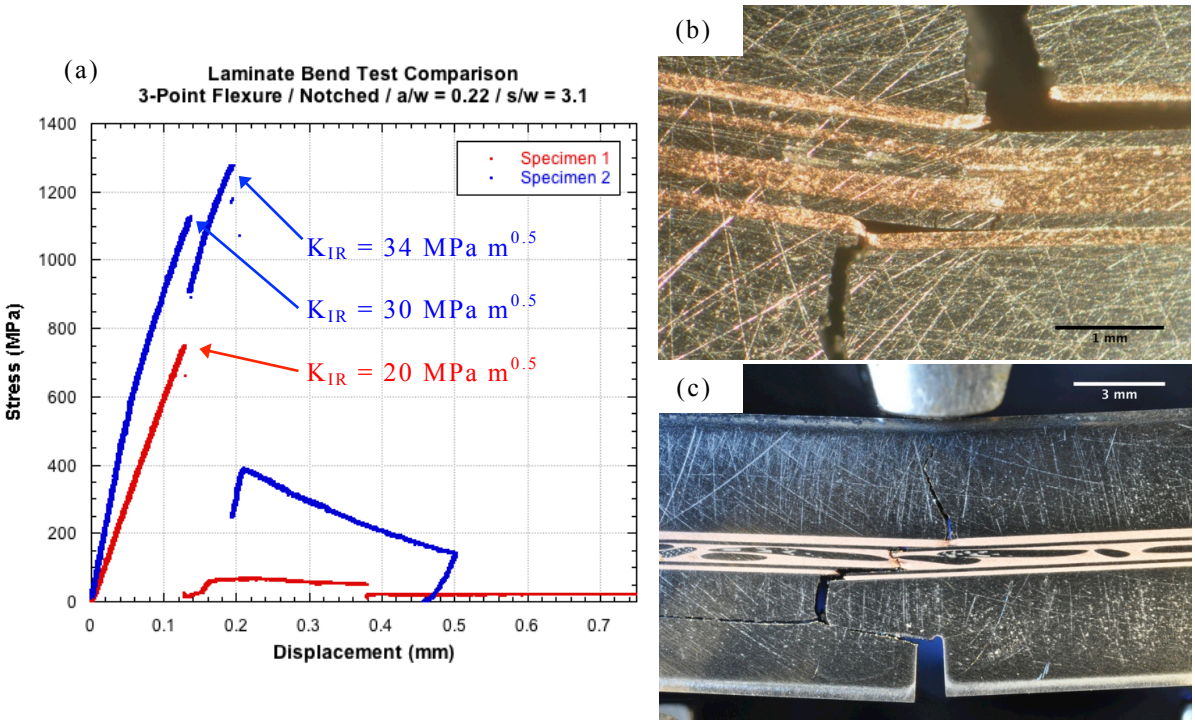

Figure 3.6. Summary of hot-pressed laminate fracture tests. a) Stress-displacement curves for two specimens are compared showing calculated stress intensity at peak load points. b) Specimen 1 after testing (notch side is bottom of image). c) Specimen 2 after testing [4].

3.4 Brazed Composites

Bend testing on the notched, non-precracked W-Cu laminate did not show pseudo-ductile behavior, but crack bridging did occur. In Figure 3.7, the dye penetrant on the fracture surface of the broken specimen indicates that when the specimen was still intact with an a/w ≈ 0.9, the Cu the reinforcement was bridging the crack. An increase in load-bearing capacity and fracture resistance is not seen in these specimens because the applied stress intensity needed to grow a sharp crack from the blunt notch tip was greater than that needed to unstably propagate a sharp dynamic crack to a/w = 0.9, since the corresponding crack opening profile does not activate a significant bridging traction.

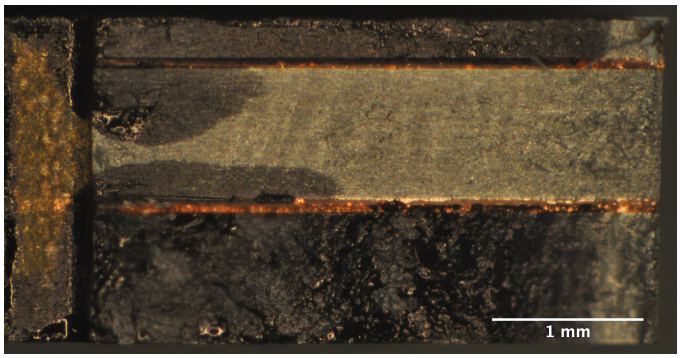

Figure 3.7. A representative fracture surface of W-Cu brazed laminate. Specimen was marked with dye penetrant at a measured a/w = 0.9 before breaking. Notch is on the left side of image. Lack of penetration through Cu layers indicates Cu was bridging the crack [5].

No face-orientation material was tested because the compression-compression precracking method caused shear failure at the W-Cu interfaces. Edge-orientation fracture was characterized by varying increments of unstable crack growth followed by crack arrest (pop-ins) due to the Cu reinforcement, as illustrated in Figure 3.8 from an L+T oriented specimen. A representative fracture surface image of a heat-tinted sample is shown in Figure 3.9 from the same L+T specimen.

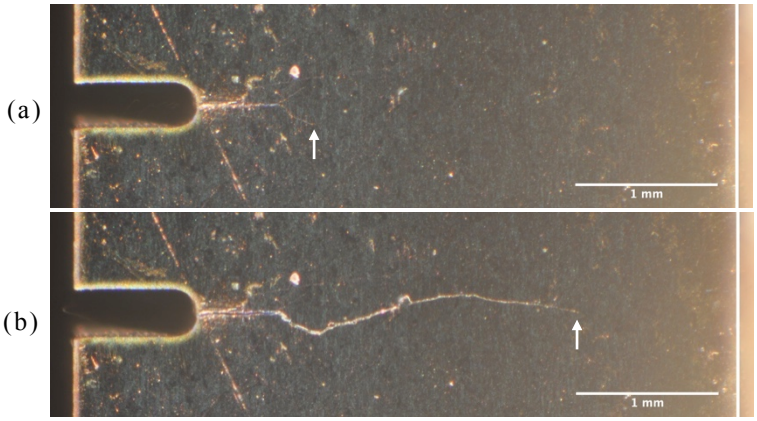

Figure 3.8. Comparison of two successive images taken during three-point bend testing on W-Cu laminate (specimen O3-2). a) The crack at a/w = 0.36 grows unstably b) to a/w = 0.76 before being arrested by the Cu reinforcement. Arrows indicate the crack tip in each image, and the vertical line at right indicates the edge of the specimen [6].

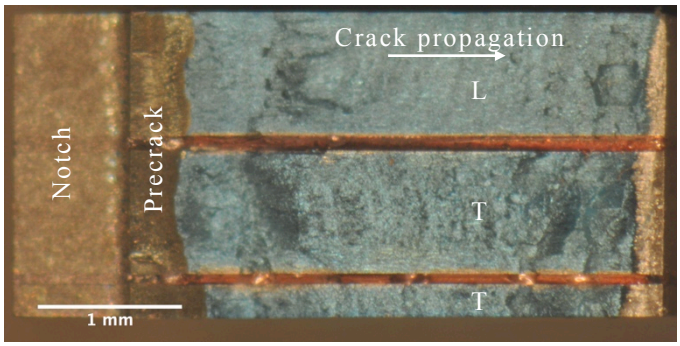

Figure 3.9. Fracture surface of W-Cu laminate bend bar (O3-2). Blue coloration on W layers is from heat tinting to observe the final crack length in different W plates. Crack is longer in L-oriented plate than in T plates. Dark contrast in blue test crack region is from surface features; L plate has relatively flat fracture surface while T plates are rough [6].

Precrack fronts had a concave or flat shape instead of the usual convex "thumbnail" shape, and in the mixed orientation the crack propagated to a greater depth in the L-oriented versus T-oriented plates. This is qualitatively consistent with the anisotropic toughness of the W matrix, as the rolled plate is tougher in the T direction than the L direction by a factor of about 1.6.

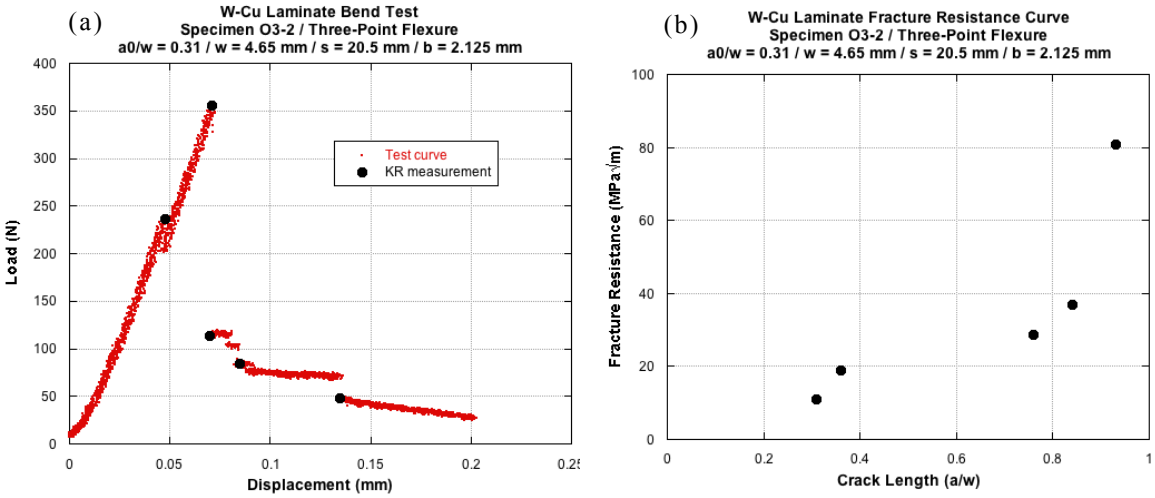

Figure 3.10. a) P-D curve and b) R-curve for W-Cu laminate bend specimen O3-2. Black points on P-D curve indicate the maximum load at each measured crack length used to calculate K_R. Significant load drops were observed corresponding to unstable crack growth and subsequent crack arrest [6].

A representative P-D curve along with the corresponding R-curve is shown in Figure 3.10, illustrating the load drops associated with unstable crack growth as well as the loads

used to calculate each point in the R-curve. A summary of all calculated R-curves is given in Figure 3.11 as a set of plots grouping tests by orientation (L, T, or L+T). The T orientation showed greater increases in toughness with crack extension than the L orientation, but had less stable crack growth.

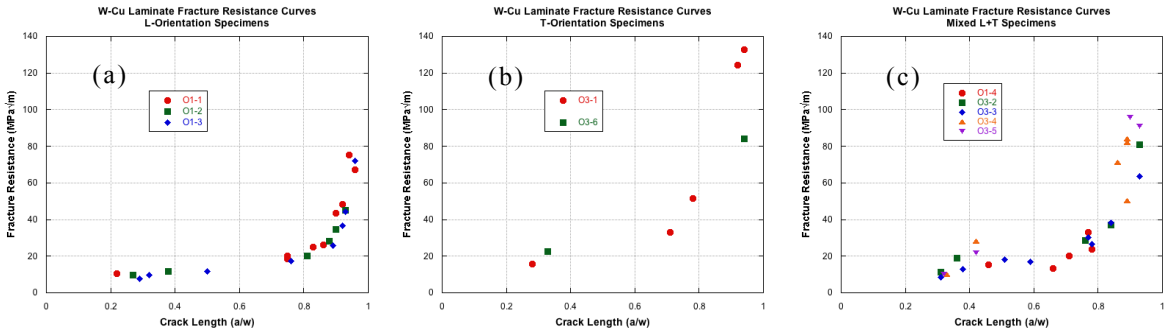

Figure 3.11. Comparison of R-curves for W-Cu laminate specimens of different orientations. Plots are grouped by specimens with a) only L-orientation W plates, b) only T-orientation plates, or c) a mix of L and T plates. The T specimens have higher initiation toughness as expected, as well as a greater increase in fracture resistance with crack growth. The L specimens show more stable crack growth, evidenced by the greater number of points per specimen. In mixed specimens, initiation toughness appears controlled by the L orientation, with the subsequent R-curve shape a mixed character of L and T [6].

For the mixed orientation, in which one of the three W plates was a different orientation than the other two (one L and two T, or vice versa), had a small initial increment of higher R-curve slope than the L orientation, but plateaued around a/w = 0.5, and reached a maximum K_{IR} between those for the L and T orientations at very large a/w. Again, this behavior simply reflects the differences in the T and L matrix toughness. These data do not show a significant difference in R-curve behavior between areas of the laminate containing 2L+1T versus 1L+2T plates.

Since the K_{IR} curves show significant toughness increases only at large a/w, one might conclude that the small amount (< 8% by volume) of relatively weak (annealed Cu) and thin reinforcement had little beneficial effects on the fracture resistance of the composite versus the monolithic W. Indeed this is the case if the metric is the relative engineering

strength of the composite. However, crack arrest and increments of quasi-stable growth are observed, providing some degree of engineering ductility in the composite that is entirely absent in the monolithic W plate. Therefore, a composite with a higher volume fraction of stronger reinforcing phase, with an optimized thickness, would be expected to perform significantly better. To this end, the crack bridging model may guide the fabrication of an improved composite.

4. Modeling Approach

In parallel with fabrication efforts, a code was developed to model ductile-phase-toughened composites. The code can accommodate any test specimen geometry for which the K_I solution is known, and may be applied to arbitrary composite architectures. The code is adapted from work by Odette and Chao on TiAl-TiNb laminates [23-25, 33].

The two major processes this code performs are: 1) predicting fracture resistance and load-displacement curves (R-curves and P-D curves), and 2) estimating the reinforcement stress-displacement function $\sigma(\Delta)$, the "bridging law." Both cases require input of the specimen geometry and matrix properties. For additional inputs, Case 1 requires the bridging law, and Case 2 requires the calculated R-curve from test data along with the measured failure displacement of the ductile ligaments.

The code was validated first by matching its Case 1 results with those published by Odette and Chao [24]. The Chao code was validated using experimental data, but only its inputs and results were available, not the program itself. The Case 2 results were validated by independently estimating the bridging laws used by the Case 1 code to create R-curves. In this way, the estimate of the bridging law could be compared to the known one.

The form of the bridging law was described with four parameters: the peak load (σ_{max}), the peak-load displacement (Δ_1), a post-peak shape exponent (n), and the failure displacement (Δ_2). A schematic of the bridging law is shown in Figure 4.1, and the role of the n parameter in defining the shape of the post-peak curve is described by Equation 4.1.

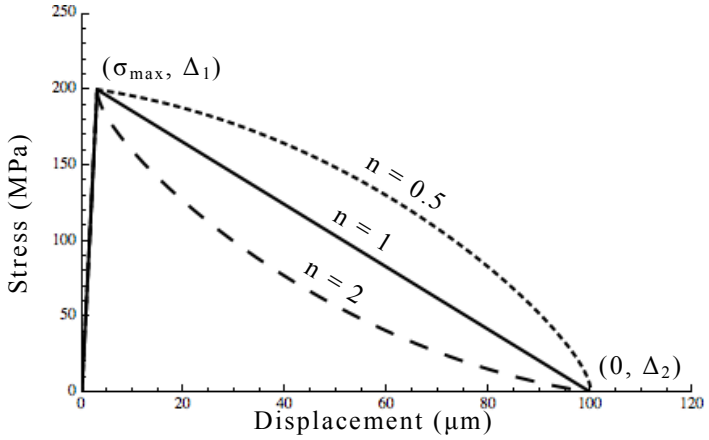

Figure 4.1. Example bridging law function. The function is defined by four parameters, and assumes linear elastic behavior approaching the peak load. Examples of the effect of n on the post-peak shape are given [7].

$$\sigma(\Delta) = \frac{\sigma_{max}}{2}\left(1-\frac{\Delta-\Delta_1}{\Delta_2-\Delta_1}\right)^n + \frac{\sigma_{max}}{2}\left(1-\left(\frac{\Delta-\Delta_1}{\Delta_2-\Delta_1}\right)^{1/n}\right), \Delta_1 < \Delta < \Delta_2 \quad [4.1]$$

A parametric study was performed by calculating R-curves and P-D curves for a matrix of various values for each bridging law parameter. The combination of parameters examined is shown in Table 4.1.

Table 4.1. Values used for each parameter in parametric study. The resulting data set contains 256 associated R-curves and P-D curves to allow for a quantitative comparison of reinforcements for a W-matrix composite [7].

σ_{max} (MPa)	100	200	300	400
Δ_1 (μm)	1	3	5	7
n	0.3	1	3	9
Δ_2 (μm)	50	150	250	350

4.1 Analytical Basis

The core mechanic of the program is an iterative calculation that generates a self-consistent solution between the bridging law [σ(Δ)], the opening displacements of the crack [Δ(x)], and the distribution of tractions along the crack face [σ(x)], as shown in Figure 4.2.

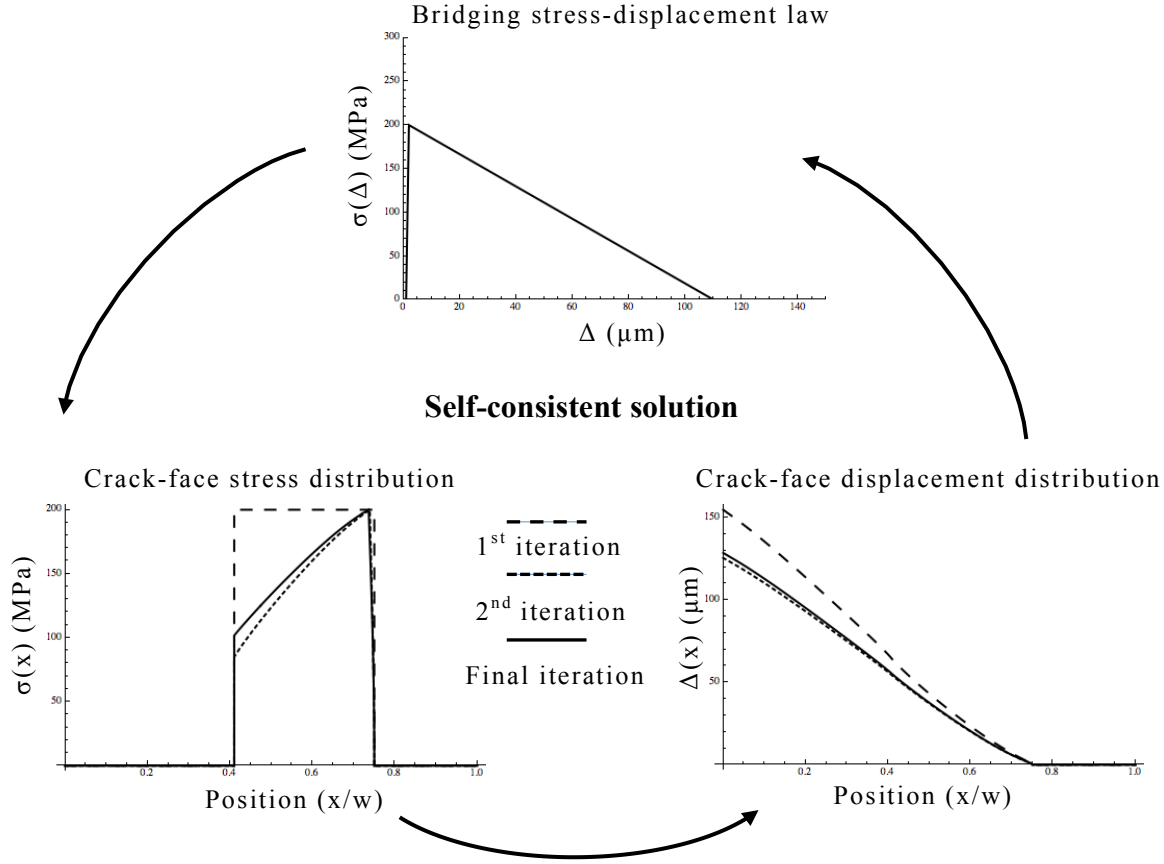

Figure 4.2. Visualization of the iterative process at the core of the large-scale bridging model.

It is assumed that the matrix crack can be described by linear elastic fracture mechanics, and that the crack is pure Mode I. Using a three-point bend specimen shown in Figure 4.3 as an example, relevant solutions are taken from Tada [34] for the stress intensity at the crack tip.

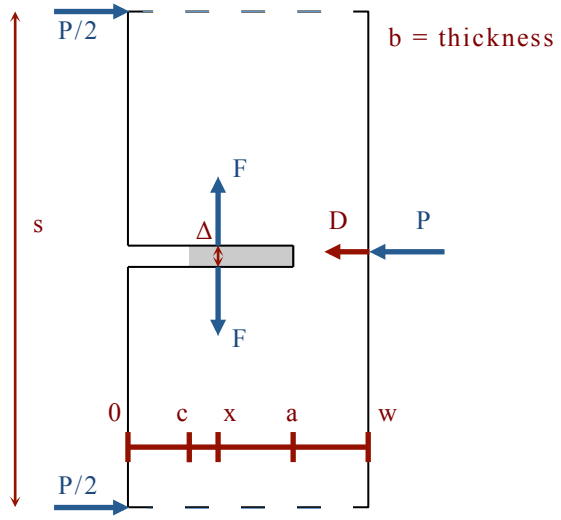

Figure 4.3. Schematic of a three-point bend specimen illustrating relevant dimensions (red) and stresses (blue). The shaded gray area represents the portion of the crack bridged by a reinforcing phase. The stresses are: the applied stress (P) and a point stress (F) at position x on the crack face. The displacements are: the crack-face displacement (Δ) at point x, and the engineering load-point displacement (D). In the x-direction, the bridging zone runs from c to the crack length a. The specimen width is w, the test span is s, and the specimen thickness (out-of-page) is b [6].

$$K_{I,P}(P,a) = \frac{3\,P\,s}{2\,w^2}\sqrt{\pi a}\,F_1\left(\frac{a}{w}\right) \qquad [4.2]$$

$$K_{I,F}(F,x,a) = \frac{2\,F}{\sqrt{\pi a}}\,F_2\left(\frac{x}{a},\frac{a}{w}\right) \qquad [4.3]$$

$K_{I,P}$ is due to the applied stress P, and $K_{I,F}$ is due to a point stress F at position x on the crack face. The functions F_1 and F_2 are shown in the appendix. The effective stress intensity at the crack tip is the applied stress intensity minus the reduction in stress intensity due to the bridging stress distribution, $K_{I,eff} = K_{I,P} - \Delta K_{I,F}$. The principle of superposition is used to treat the bridging zone tractions as a series of point forces along the crack face, and $\Delta K_{I,F}$ is found by integrating over the bridging zone.

$$\Delta K_{I,F} = \int_0^a K_{I,F}[\sigma(x),x,a]\,dx \qquad [4.4]$$

The applied stress intensity reaches its critical value, the composite fracture resistance, ($K_{I,P} = K_{IR}$) when the effective stress intensity at the crack tip is equal to the matrix toughness ($K_{I,eff} = K_{IC}$), thus

$$K_{IR} = \Delta K_{I,F} + K_{IC}. \quad [4.5]$$

Once the fracture resistance has been calculated, Castigliano's Theorem is applied to calculate the shape of the crack. Castigliano's Theorem states that the displacement due to a force Q in the direction of that force is equal to the partial differential of the total strain energy with respect to that force [34].

$$\Delta_Q = \frac{\partial U_T}{\partial Q} \quad [4.6]$$

The strain energy may be separated into two components: the strain energy of the uncracked body, and the additional energy due to introducing the crack while holding the forces constant [34]:

$$U_T = U_{nc} + \int_0^A \frac{\partial U_T}{\partial A} dA. \quad [4.7]$$

Substitute into Castigliano's Theorem to derive the displacements of the uncracked and cracked bodies, where the uncracked displacement is identically zero at the crack face. Also, substitute the energy release rate G_I for $\frac{\partial U_T}{\partial A}$ [34].

$$\Delta_Q = \frac{\partial U_{nc}}{\partial Q} + \frac{\partial}{\partial Q}\int_0^A G_I dA = \frac{\partial}{\partial Q}\int_0^A G_I dA \quad [4.8]$$

From Irwin's relationship, and assuming a Mode I crack [34],

$$E' G_I = {K_I}^2 = \left(K_{I,P} + K_{I,F}\right)^2. \quad [4.9]$$

Combining Equations 4.8 and 4.9 and allowing the virtual forces to approach zero, solutions are found for the opening and closing displacements, Δ_P and Δ_F. The net displacement Δ is the difference between the two [33].

$$\Delta_P(x) = \frac{2}{E'}\int_x^a K_{IP}(P, a')\frac{\partial K_{IF}(F,x,a')}{\partial F}da' \quad [4.10]$$

$$\Delta_F(x) = \frac{2}{E'}\int_x^a\left[\int_0^{a'} K_{IF}(\sigma(x'), x', a')dx'\right]\frac{\partial K_{IF}(F,x,a')}{\partial F}da' \quad [4.11]$$

$$\Delta(x) = \Delta_P(x) - \Delta_F(x) \quad [4.12]$$

In both cases, the integrand consists of the stress intensity due to the opening or closing tractions at the instantaneous crack length a', multiplied by the partial derivative of the crack-face $K_{I,F}$ with respect to F. In the calculation of Δ_F, the stress intensity due to the bridging tractions at an instantaneous crack length a' is itself an integrated quantity, similar to $\Delta K_{I,F}$.

Finally, the load-point displacement is calculated as the elastic solution minus the contribution from the bridging zone. The former is given by Timoshenko and Tada, and the latter follows the above derivation applied to the case of displacements in the direction of P. The resulting solutions for the reduction in displacement due to the bridging zone (D_F), and the net displacement (D) are [33-34]

$$D_F = \frac{2}{E'}\int_0^a\left[\int_0^{a'} K_{IF}(x, a')dx\right]\frac{\partial K_{IP}(a')}{\partial P}da' \quad [4.13]$$

$$D = P\left(\frac{s^3}{4E'w^3} + \frac{s}{2w}\left(\frac{3}{4G} - \frac{3}{10E'} - \frac{3\nu}{4E'}\right) - \frac{0.21}{E'}\right) + \frac{3Ps^2}{2E'w^2}V_2\left(\frac{a}{w}\right) - D_F \quad [4.14]$$

where the function V_2 is defined in the appendix.

4.2 Procedural Structure

4.2.1 Determination of R-Curves and P-D Curves

Input data. Enter the specimen dimensions (width, span, thickness, precrack depth), matrix properties (Young's modulus, Poisson's ratio, fracture toughness), and bridging law (can be defined as any continuous function). A shape function may be used to define any

discontinuities the crack front would encounter while propagating through the material (such as with a face-orientation laminate specimen). Specify the calculation parameters – crack growth step size and convergence criteria [$\sigma(x)$ and bridging zone length].

Define functions. Set up functions that will be called often in the code, and create variable arrays that will be used to track the solutions for each step of the calculation.

Calculate the applied load needed to advance the crack. Start by growing the crack from its initial depth to the next increment, and assume that region to be the current bridging zone. Assume a constant stress over the bridging zone and calculate $\Delta K_{I,F}$ from that $\sigma(x)$. Then calculate K_{IR} and use the form of $K_{I,P}$ to find P.

Calculate the shape of the crack. Define a mesh of points on the crack face. Calculate the opening, closing, and net crack-face displacement at each point.

Update the bridging traction guess. Use the bridging law to calculate the stress corresponding to each crack-face displacement and interpolate over the mesh to update the guessed bridging stress distribution. Calculate the difference between the two stress distributions by taking the sum of the absolute difference at each point in the mesh. If the error is below the convergence criterion, accept the solution; otherwise, repeat the calculation with the updated $\sigma(x)$. After checking the convergence of the stress distribution, check the convergence of the bridging zone length. Repeat if the change in bridging zone size does not satisfy the convergence criterion. Once all calculations have converged, continue to the next crack length. Stop before the virtual crack grows past the width of the specimen.

Calculate the load-point displacements. Recall the $\sigma(x)$ and other solutions from the first iteration of crack length extension. Calculate the elastic load-point displacement for

that crack length and the reduction in displacement due to the bridging zone. Repeat for each value of crack length.

When the algorithm has finished running, the solutions for $\sigma(x)$, $\Delta(x)$, K_{IR}, P, and D are all stored in arrays according to which crack length they correspond to. The evolution of each parameter may be visualized graphically, and of course the R-curve and P-D curve may be plotted. R-curves are plotted as K_{IR} in MPa vs. normalized crack length (a/w). P-D curves are plotted as P/P' vs. D/D', where P' and D' are the elastic failure load and displacement of a pure-matrix specimen of the same geometry.

4.2.2 Determination of Bridging Law

Input data. Specify the same inputs as above with the following exceptions. Enter the R-curve data. Enter the bridging law parameters. As the parameters are not known except for the failure displacement Δ_2, enter initial guess values for σ_{max}, Δ_1, and n. The guess for Δ_1 should be small for the prediction to be most accurate. Define a step size for guesses in Δ_1, convergence criteria for the calculation of σ_{max} and n, and a gain value to help the n solution converge in fewer iterations. Store the R-curve as an interpolated function. A step size for crack growth is not necessary for this calculation.

Define functions. The set of functions to call during the calculation is the same. The set of empty lists is also the same with the addition of lists to hold the solutions for σ_{max}, Δ_1, and n after each iteration.

Estimate Δ_1 and σ_{max} simultaneously. Model a short crack extension ($a - a_0$). Use the elastic near-tip crack shape solution to solve for this crack length from a given Δ_1 [34].

$$\Delta = \frac{4\sqrt{2}}{\sqrt{\pi}E'} K_{IC}\sqrt{a - a_0} \quad \rightarrow \quad a = a_0 + \left(\frac{\Delta_1\sqrt{\pi}E'}{4K_{IC}\sqrt{2}}\right)^2 \qquad [4.15]$$

This method ensures that at no point in the bridging zone will $\Delta(x) > \Delta_1$; thus, the activated region of the bridging law will always be within the guessed elastic region and the post-peak shape has no effect. Use the guess value for σ_{max} as the constant-stress $\sigma(x)$ guess.

Proceed with the calculation of $\Delta K_{I,F}$ as in Case 1. Then use the known K_{IR} value for this crack length (from the interpolation of the R-curve data) to calculate the true $\Delta K_{I,F}$. Scale the guessed $\sigma(x)$ distribution as well as the σ_{max} guess by the ratio of the true $\Delta K_{I,F}$ to the initial guess, ensuring that the calculated K_{IR} value is correct, and proceed using the scaled $\sigma(x)$. Proceed as in Case 1 to calculate the crack shape and update the stress distribution, and then repeat the process until the change in the estimated σ_{max} satisfies the convergence criterion.

Accept this estimate of σ_{max} for the given crack length, then increase by one step in Δ_1, recalculate the corresponding crack length, and repeat to estimate a series of (Δ_1,σ_{max}) points. The resulting set of estimates looks like an approximation to the elastic portion of the bridging law. Stop increasing Δ_1 once the convergent σ_{max} value is lower than that for the previous Δ_1 step. Finally, choose from these points the best estimate of (Δ_1, σ_{max}).

Figure 4.4 explains the best-estimate selection process graphically. The current strategy is to find the point at which the estimated (Δ_1, σ_{max}) curve deviates from linearity. To do this, fit a series of linear regressions to the data, removing the last point with each successive fit (start with the blue fit in Fig. 4.4a). Analyze the list of goodness-of-fit values (R^2) from each linear regression to find the index of first local maximum (red circle in Fig. 4.4b). This index corresponds to the best estimate of Δ_1 and σ_{max} (red circle in Fig. 4.4a).

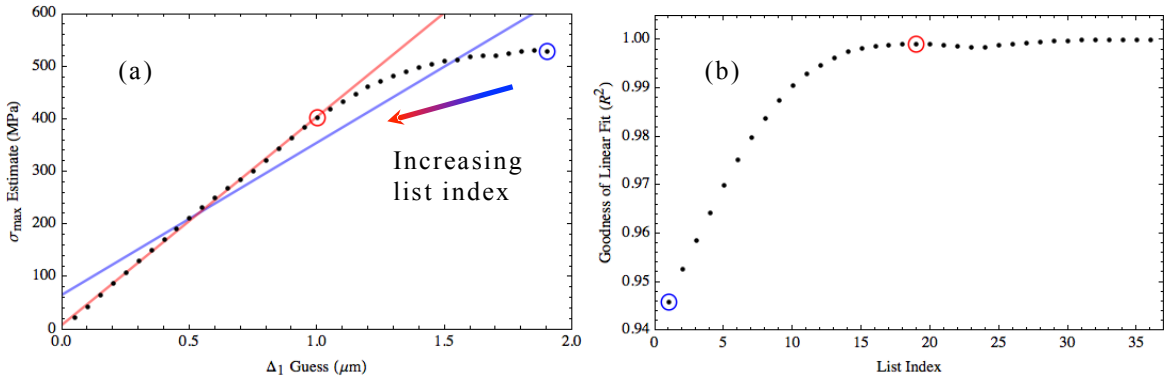

Figure 4.4. a) Plot of estimated (Δ_1, σ_{max}) points showing the first (blue) and the best-guess (red) linear fits. Colored circles around points indicate the highest Δ_1 value used in the corresponding fit. The best-guess (Δ_1, σ_{max}) point (red circle) is taken as the final estimate for the two parameters. b) Plot of goodness-of-fit value (R^2) for each linear regression vs. the list index as shown in Fig. 4.4a. Blue and red circles indicate the R^2 values corresponding to the fits shown in Fig. 4.4a. The best guess is selected by finding the first local maximum in R^2 (red circle).

Estimate the post-peak shape parameter. At this point, the other three parameters are known and only the guess value for n remains. Calculate an R-curve using the current bridging law guess. In calculating the R-curve, use the same crack length values as those measured in the true R-curve data. Integrate each R-curve with respect to crack length and compare the respective area under each curve. Update the guess value for n,

$$n_i = n_{i-1}\left[\frac{\int K_{IR,guess}(a)\,da}{\int K_{IR,true}(a)\,da}\right]^z, \qquad [4.16]$$

where z is a gain exponent that accelerates convergence. Continue iterating until the change in n satisfies the convergence criterion.

5. Model Results

5.1 Determination of R-Curves and P-D Curves

The large-scale crack bridging code results were compared the previous work of Odette and Chao [24], since that work was validated experimentally. Figure 5.1 shows resistance curves and load-displacement curves calculated for three different bridging stress-

displacement functions, indicated by color. The new resistance curve calculations (points) compare very well with the previous results (lines) but the P-D predictions are only consistent up to nearly the peak load. After the peak load, the load-point displacement is under-predicted with respect to the previous results. The calculation converges quickly when modeling specimens in the edge orientation because the reinforcement is continuous in the direction of crack propagation. Additional meshing steps are required for accurate face-orientation modeling.

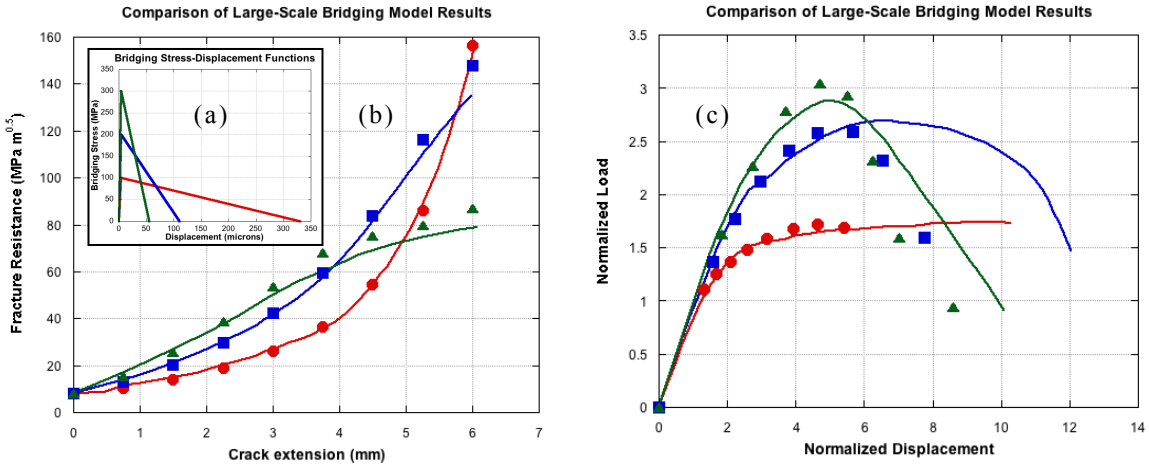

Figure 5.1. Experimentally-verified models (lines) compared with current models (points) for identical initial conditions, modeling a TiAl-TiNb laminate. a) Bridging law functions corresponding to the colors in each plot. b) Comparison of resistance curves. c) Comparison of load-displacement curves. Values are normalized by the load capacity and displacement at fracture of a non-reinforced test specimen [5, 24].

5.2 Determination of Bridging Law

It is generally not possible to directly measure $\sigma(\Delta)$ curves for embedded reinforcements since this depends on details like debonding and triaxial stresses in matrix cracks that are blunted in the ductile phase. However, as noted above they can be inversely extracted from test data. The estimation strategy for σ_{max} and Δ_1 successfully reconstructed the elastic loading portion of the bridging law as shown in Figure 5.2a. The estimate for n

also converges near enough to the true value (Fig. 5.2b) that the R-curve fits well with the input data (Fig. 5.2c).

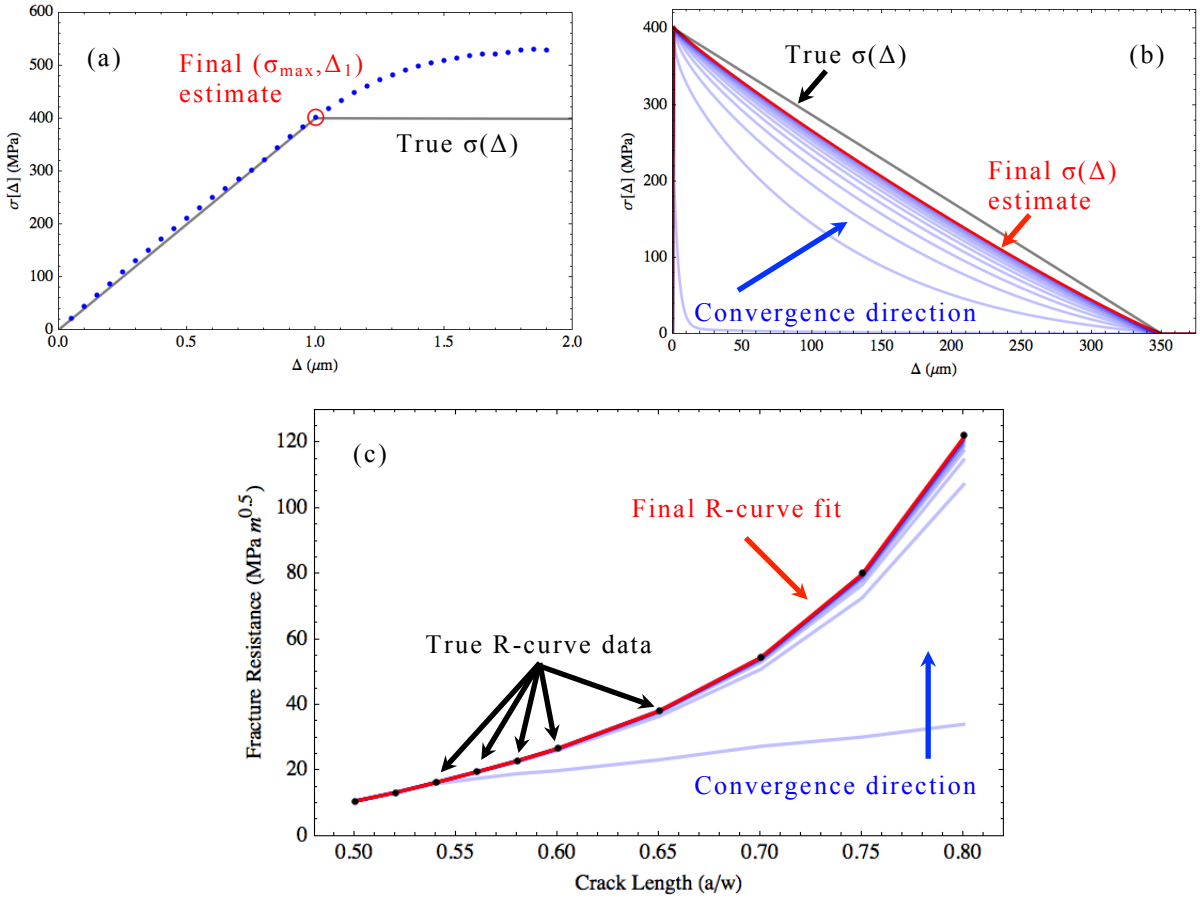

Figure 5.2. a) Estimate of (σ_{max},Δ_1) point (red circle) shown against a close-up view of the true bridging law (gray curve). Calculated values (points) track well with the elastic slope of the bridging law. b) Estimate of n parameter shown as a series of calculated bridging laws (blue curves), highlighting final estimate (red curve). Compare to the true bridging law (gray curve). c) Black points show the true R-curve. Blue curves show successive iterations during estimation of n, and red curve corresponds to the final bridging law estimate.

5.3 Parametric Study

A parametric study of reinforcement σ(Δ) was used to evaluate the effects of the controlling parameters individually and in combination as illustrated in Figure 5.3. Here the P-D curves are normalized by the corresponding loads and displacements at elastic fracture of the brittle matrix, P' and D', respectively.

σ_{max} [MPa]	Δ_1 [μm]	n -	Δ_2 [μm]	P-D Curves [P/P' vs. D/D']	R-Curves [K_{IR} (MPa) vs. a/w]
100 200 300 400	1	0.3	350	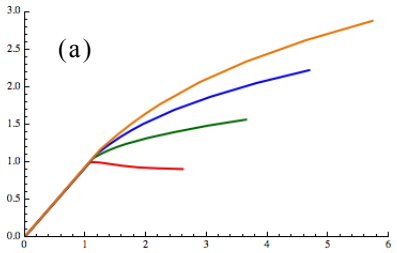	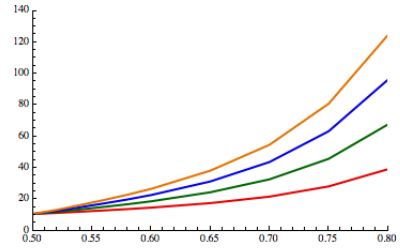
400	1 3 5 7	0.3	350	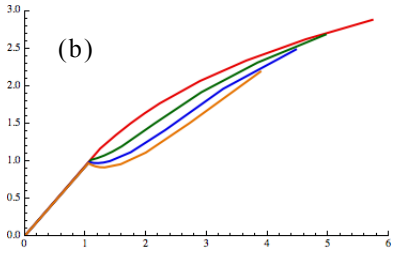	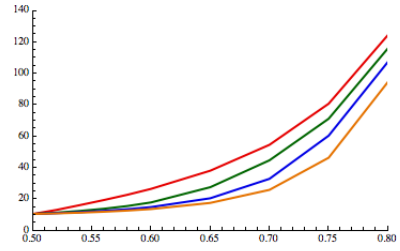
400	1	0.3 1 3 9	350	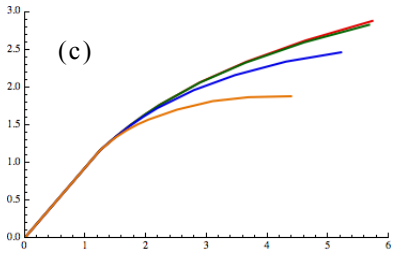	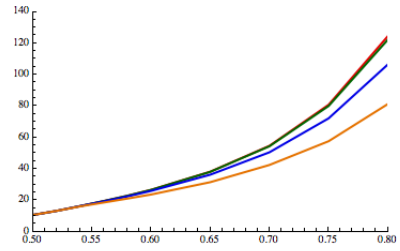
400	1	9	50 150 250 350	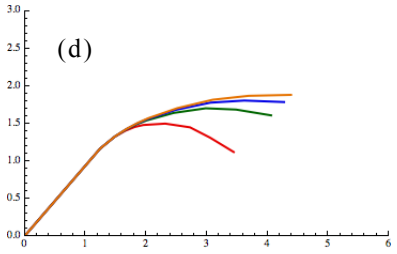	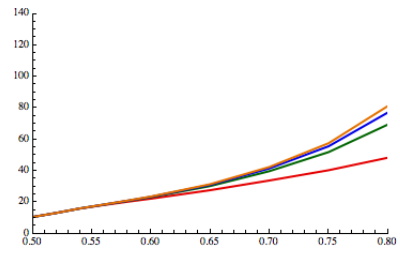

Figure 5.3. Parametric study summary. In each row of values and plots, one parameter is varied and the resulting P-D curves and R-curves are shown. Load and displacement values are normalized by the load capacity (P') and displacement (D') at fracture, respectively, of the unreinforced tungsten matrix. The mechanical behavior of the composite is more sensitive to σ_{max} and u_1 than to n and u_2 [6].

For a desirable, and expected, low value of Δ_1, the P-D and K_{IR}(a/w) curves increase with increasing σ_{max}, resulting in a desirable increase in P_{max}, accompanied by increasing D or ductility (Fig. 5.3a). The detrimental effect of increasing Δ_1 is also revealed in the P-D curves (Fig. 5.3b). Both increasing the convex shape of the bridging law (Fig. 5.3c) and, to a lesser extent, increasing Δ_2 (Fig. 5.3d) increase the composite strength and ductility.

It must be emphasized that while these effects can be qualitatively anticipated, they all represent large-scale bridging effects for a growing bridging zone that cannot be quantitatively predicted based on intuition or simple energy-based concepts. The engineering performance capabilities of a DPT composite are reflected in the normalized P-D curves with values of P/P' and D/D' greater than 1, which is the limit for the elastically brittle monolithic matrix material. It is also worth noting that it is the initial slope of the R-curve that controls the crack growth initiation P-D and any subsequent stable crack growth for any expected practical initial crack length.

6. Discussion and Conclusions

The goal of this work was to demonstrate ductile-phase toughening in a tungsten composite. Early work to develop composites with spark plasma sintering or hot pressing fabrication routes were unsuccessful in terms of enabling stable crack growth through crack bridging; however, a brazed W-Cu laminate demonstrated these properties in fracture testing. A large-scale crack bridging model was developed to predict mechanical properties of an arbitrary composite or its reinforcing phase.

The EBSD data collected to analyze the microstructure evolution in W wire during processing is limited but may indicate the beginning of recrystallization at high temperature of the highly-deformed wire. The extrinsic toughening at installation of a DPT W composite will indeed come from a ductile reinforcement, but more investigation is required to understand whether these reinforcements will continue to provide such toughening by the end of the material's service life. The dominant mechanism may shift from deformation of the reinforcement to frictional sliding during pull-out, for example.

The toughness of the W plates is higher than the expected value for the as-sintered material, due to severe plastic deformation during the rolling process. However, considering the large-scale material demand for a fusion reactor, such processed forms of W should not be relied upon for composite research without a thorough investigation of the economics of scale for such processes. Generally speaking, the simplest processing route to a toughened composite should be pursued.

Sintering of W powders in this study resulted in greater than 95% densification. A 2-temperature sintering route to consolidate W around Cu-coated W wires is unlikely to be effective unless full matrix densification occurs at the low temperature. The pulsed current capabilities of the SPS have not been explored here, but may be useful in this effort.

Besides tungsten, carbon is the most favorable element for high-temperature use in a divertor application. The previous plan for ITER was to begin operation using a divertor with both carbon-carbon composite and W armor components before switching to full W – this plan was changed in favor of using only W from the beginning due to cost concerns. It must be noted that a fully carbon divertor gives rise to significant tritium retention issues, so minimizing the fraction of carbon in a W-composite debonding layer is a key concern [35]. In this study, tungsten carbide as an interface layer was too strongly bonded to the matrix to give rise to any crack bridging. Fugitive interfaces are a possible design choice in this case, where porosity is introduced at the interface [36]. This utility in aiding debonding must be balanced with thermal conductivity needs.

The complexity of the hot-pressed laminate material may not be amenable to large-scale processing. The general concept of embedding W wires in a W matrix, however, is still an intriguing one. Some evidence of fiber pullout was observed in tests on the hot-pressed

laminate, and the embedded "sandwich" reinforcement was able to arrest the crack. A finer-scale laminate may allow for greater stable crack growth normal to the layers. Additionally, controlled precracking is vital for R-curve testing on W composites.

Ductile-phase toughening has been demonstrated for W plates brazed with Cu. Stronger reinforcements are needed to give an increased engineering strength, but even a weak reinforcement enabled crack arrest and significant ductility. While Cu is useful for developing model composites, it is not a viable choice for PFCs [26]. Further development should focus on acceptable elements.

The large-scale bridging model is a powerful tool for composite design and analysis. While in this study the possible composite architectures were constrained by available equipment, future fabrication efforts may choose processes better suited to working with, for example, larger and more ordered layups of coated W fibers. A parametric study of reinforcement bridging laws applied to a matrix of interest can guide the initial selection of reinforcement material and the required volume fraction of reinforcement. After preliminary R-curve testing, the actual bridging law for the new material may be derived using the model and then used to refine the composite design.

The calculation of R-curves is robust, but displacement calculations are too conservative in comparison to the previous model. The reduction in load-point displacement due to the bridging zone is calculated to be greater in the current code than in the previous one. This discrepancy may arise from a difference in the integration strategies used by each code. The algorithm for determining bridging laws is robust in its estimate of σ_{max} and Δ_1, and while errors remain in the estimation of n, the calculated R-curve is not sensitive to this

error. An improved code would include a more adaptive convergence algorithm for determining n, as well as estimation strategies for Δ_2 and potentially the residual stress.

7. Recommendations for Future Work

Development of W-composite PFCs must be guided by the evolving thermal and mechanical requirements for divertor components. Broadly, the three aspects of W-composite PFC development are the choice of reinforcement material and architecture, optimization of the fabrication route, and control of in-service microstructure evolution.

Efforts should be made to develop scalable fabrication routes for near-net-shape W-composite parts by pairing rapid consolidation techniques like SPS with fiber layup tools and green body forming techniques like powder-injection molding [12, 37]. Sintering around a preform can result in matrix cracking to relieve stress during consolidation, but this process could be useful for extrinsic toughening if a weak interface layer was designed to crack instead of the matrix [38]. The utility of a composite for large-scale application depends strongly on economy of fabrication, so it is helpful to design materials with this in mind. The availability of W product forms (wire, foil, plate, etc.) for large-scale composite fabrication should also be considered. For composite layups there is a need for appropriate tooling, such as near-net-shape sintering dies and fiber alignment tools.

Structural tungsten components remain a critical research need for the future of fusion energy. The next steps in developing DPT tungsten should involve choosing reinforcements that are compatible with the divertor environment. Low-activation elements include Fe, Cr, V, Ti, Si, and C [26]. Experimentation and modeling should proceed together in an iterative design process.

References

[1] C. H. Henager, R. J. Kurtz, G. R. Odette, and F. W. Zok, "Ductile-phase toughened and fiber-reinforced tungsten for plasma facing materials," Proposal to the U.S. Department of Energy Office of Science, Fusion Energy Sciences. Materials solicitation with focus on structural materials, blanket first walls, and divertor plasma facing components, 2011.

[2] K. H. Cunningham, K. Fields, D. Gragg, F. W. Zok, C. H. Henager, Jr., R. J. Kurtz, and T. Roosendaal, "Recent progress in the development of ductile-phase-toughened tungsten for plasma-facing materials," in DOE/ER-0313/54 - Volume 54, Semiannual Progress Report, June 30, 2013. 2013, US DOE: ORNL, TN.

[3] C. H. Henager, Jr., R. J. Kurtz, T. J. Roosendaal, B. A. Borlaug, G. R. Odette, K. H. Cunningham, K. Fields, D. Gragg, and F. W. Zok, "Recent progress in the development of ductile-phase-toughened tungsten for plasma-facing materials," in DOE/ER-0313/55 - Volume 55, Semiannual Progress Report, Dec. 31, 2013. 2013, US DOE: ORNL, TN.

[4] K. H. Cunningham, G. R. Odette, K. Fields, D. Gragg, F. W. Zok, C. H. Henager, Jr., R. J. Kurtz, T. J. Roosendaal, and B. A. Borlaug, "Recent progress in the fabrication and characterization of ductile-phase-toughened tungsten composites for plasma-facing materials," in DOE/ER-0313/56 - Volume 56, Semiannual Progress Report, Jun. 30, 2014. 2014, US DOE: ORNL, TN.

[5] K. H. Cunningham, G. R. Odette, K. Fields, D. Gragg, T. Yamamoto, F. W. Zok, C. H. Henager, Jr., R. J. Kurtz, T. J. Roosendaal, and B. A. Borlaug, "Recent progress in the fabrication and characterization of ductile-phase-toughened tungsten laminates for plasma-facing materials," in DOE/ER-0313/57 - Volume 57, Semiannual Progress Report, Dec. 31, 2014. 2014, US DOE: ORNL, TN.

[6] K. H. Cunningham, G. R. Odette, K. Fields, D. Gragg, T. Yamamoto, and F. W. Zok, "Recent progress in the fabrication and characterization of ductile-phase-toughened tungsten laminates for plasma-facing materials," in DOE/ER-0313/58 - Volume 58, Semiannual Progress Report, Jun. 30, 2015. 2015, US DOE: ORNL, TN.

[7] M. Rieth, J. L. Boutard, S. L. Dudarev, T. Ahlgren, S. Antusch, N. Baluc, M. F. Barthe, C. S. Becquart, L. Ciupinski, J. B. Correia, C. Domain, J. Fikar, E. Fortuna, C. C. Fu, E. Gaganidze, T. L. Galán, C. García-Rosales, B. Gludovatz, H. Greuner, K. Heinola, N. Holstein, N. Juslin, F. Koch, W. Krauss, K. J. Kurzydlowski, J. Linke, C. Linsmeier, N. Luzginova, H. Maier, M.S. Martínez, J. M. Missiaen, M. Muhammed, A. Muñoz, M. Muzyk, K. Nordlund, D. Nguyen-Manh, P. Norajitra, J. Opschoor, G. Pintsuk, R. Pippan, G. Ritz, L. Romaner, D. Rupp, R. Schaublin, J. Schlosser, I. Uytdenhouwen, J. G. Van Der Laan, L. Veleva, L. Ventelon, S. Wahlberg, F. Willaime, S. Wurster, and M. A. Yar, "Review on the EFDA programme on tungsten materials technology and science," *Journal of Nuclear Materials* **417**, 463-467 (2011).

[8] R. A. Pitts, A. Kukushkin, A. Loarte, A. Martin, M. Merola, C. E. Kessel, V. Komarov, and M. Shimada, "Status and physics basis of the ITER divertor," *Physica Scripta* **T138**, 014001 (2009).

[9] P. Mertens, T. Hirai, M. Knaup, O. Neubauer, V. Philipps, J. Rapp, V. Riccardo, S. Sadakov, B. Schweer, A. Terra, I. Uytdenhouwen, and U. Samm, "A bulk tungsten divertor row for the outer strike point in JET," *Fusion Engineering and Design* **84**(7-11), 1289-93 (2009).

[10] A. Gervash, R. Giniyatulin, T. Ihli, W. Krauss, A. Makhankov, I. Mazul, P. Norajitra, and N. Yablokov, "Fabrication of a He-cooled divertor module for DEMO reactor," *Journal of Nuclear Materials* **367-370**, 1472-1475 (2007).

[11] M. Merola, W. Danner, and M. Pick, "EU R&D on divertor components," *Fusion Engineering and Design* **75-79**, 325-331 (2005).

[12] M. Merola, F. Escourbiac, A. R. Raffray, P. Chappuis, T. Hirai, S. Gicquel, the ITER Blanket and Divertor Sections procuring Domestic Agencies, and the Blanket Integrated Product Team, "Engineering challenges and development of the ITER Blanket System and Divertor," *Fusion Engineering and Design* (2015), DOI: 10.1016/j.fusengdes.2015.06.045.

[13] M. Rieth, S. L. Dudarev, S. M. Gonzalez de Vicente, J. Aktaa, T. Ahlgren, S. Antusch, D. E. J. Armstrong, M. Balden, N. Baluc, M.-F. Barthe, W. W. Basuki, M. Battabyal, C. S. Becquart, D. Blagoeva, H. Boldyryeva, J. Brinkmann, M. Celino, L. Ciupinski, J.B. Correiam, A. De Backer, C. Domain, E. Gaganidze, C. García-Rosales, J. Gibson, M.R. Gilbert, S. Giusepponi, B. Gludovatz, H. Greuner, K. Heinola, T. Höschen, A. Hoffmann, N. Holstein, F. Koch, W. Krauss, H. Li, S. Lindig, J. Linke, Ch. Linsmeier, P. López-Ruiz, H. Maier, J. Matejicek, T.P. Mishra, M. Muhammedl, A. Muñoz, M. Muzyk, K. Nordlund, D. Nguyen-Manh, J. Opschoor, N. Ordás, T. Palacios, G. Pintsuk, R. Pippan, J. Reiser, J. Riesch, S.G. Roberts, L. Romaner, M. Rosiński, M. Sanchez, W. Schulmeyer, H. Traxler, A. Ureña, J.G. van der Laan, L. Veleva, S. Wahlberg, M. Walter, T. Weber, T. Weitkamp, S. Wurster, M.A. Yar, J.H. You, and A. Zivelonghi, "Recent progress in research on tungsten materials for nuclear fusion applications in Europe," *Journal of Nuclear Materials* **432**, 482-500 (2013).

[14] P. Mertens, V. Philipps, G. Pintsuk, V. Riccardo, U. Samm, V. Thompson, and I. Uytdenhouwen, "Clamping of solid tungsten components for the bulk W divertor row in JET-precautionary design for a brittle material," *Physica Scripta* **T138**, 014032 (2009).

[15] B. Gludovatz, S. Wurster, A. Hoffmann, and R. Pippan, "Fracture toughness of polycrystalline tungsten alloys," *International Journal of Refractory Metals and Hard Materials* **28**(6), 674-8 (2010).

[16] S. J. Zinkle and N. M. Ghoniem, "Operating temperature windows for fusion reactor structural materials," *Fusion Engineering and Design* **51-52**, 55-71 (2000).

[17] M. Faleschini, H. Kreuzer, D. Kiener, and R. Pippan, "Fracture toughness investigations of tungsten alloys and SPD tungsten alloys," *Journal of Nuclear Materials* **367-370**, 800-805 (2007).

[18] T. Tanno, A. Hasegawa, J. C. He, M. Fujiwara, M. Satou, S. Nogami, K. Abe, and T. Shishido, "Effects of transmutation elements on the microstructural evolution and electrical resistivity of neutron-irradiated tungsten," *Journal of Nuclear Materials* **386-388**, 218-221 (2009).

[19] T. Tanno, A. Hasegawa, M. Fujiwara, H. Jian-Chao, S. Nogami, M. Satou, T. Shishido, and K. Abe, "Precipitation of solid transmutation elements in irradiated tungsten alloys," *Materials Transactions* **49**(10), 2259-64 (2008).

[20] T. Tanno, A. Hasegawa, H. Jian-Chao, M. Fujiwara, S. Nogami, M. Satou, T. Shishido, and K. Abe, "Effects of transmutation elements on neutron irradiation hardening of tungsten," *Materials Transactions* **48**(9), 2399-402 (2007).

[21] J. Riesch, T. Höschen, C. Linsmeier, S. Wurster, and J.-H. You, "Enhanced toughness and stable crack propagation in a novel tungsten fibre-reinforced tungsten composite produced by chemical vapour infiltration," *Physica Scripta* **T159**, 014031 (2014).

[22] P. R. Subramanian and D. E. Laughlin, "Cu-W (Copper-Tungsten)," in monograph, "Phase diagrams of binary tungsten alloys," ed. S. V. N. Naidu and P. R. Rao, Indian Institute of Metals, Calcutta, 76-79 (1991).

[23] R. Venkateswara, G. R. Odette, and R. O. Ritchie, "Ductile-reinforcement toughening in TiAl intermetallic-matrix composites: Effects on fracture toughness and fatigue-crack propagation resistance," *Acta Metallurgica et Materialia* **42**(3), 893-911 (1994).

[24] G. R. Odette, B. L. Chao, J. W. Sheckherd, and G. E. Lucas, "Ductile phase toughening mechanisms in a TiAl-TiNb laminate composite," *Acta Metallurgica et Materialia* **40**(9), 2381-9 (1992).

[25] J. A. Heathcote, "The fracture behavior of intermetallic/metallic microlaminate composites," Ph.D. Dissertation, University of California, Santa Barbara, 1996.

[26] N. Baluc, "Material degradation under DEMO relevant neutron fluences," *Physica Scripta* **T138**, 014004 (2009).

[27] I. Charit, D. P. Butt, M. Frary, and M. C. Carroll, "Fabrication of tungsten-rhenium cladding materials via spark plasma sintering for ultra high temperature reactor applications," U.S. Department of Energy (FY2009 NE-UP Program), 10/1/2009 to 9/30/2012.

[28] K. Williams and R. S. Muller, "Etch rates for micromachining processing," *Journal of Microelectromechanical Systems* **5**(4), 256-269 (1996).

[29] ASTM Standard B322, 1999 (2009), "Guide for cleaning metals prior to electroplating," ASTM International, West Conshohocken, PA, DOI: 10.1520/B0322-99R09.

[30] ASTM Standard B482, 1985 (2008), "Practice for preparation of tungsten and tungsten alloys for electroplating," ASTM International, West Conshohocken, PA, 10.1520/B0482-85R08.

[31] I. S. Mahmoud, "Copper plating bath and process for difficult to plate metals." Patent 4,990,224. 5 February 1991.

[32] ASTM Standard B322, 2012, "Standard test method for linear-elastic plane-strain fracture toughness K_{IC} of metallic materials," ASTM International, West Conshohocken, PA, DOI: 10.1520/E0399-12.

[33] G. R. Odette and B. L. Chao, unpublished notes.

[34] H. Tada, P. C. Paris, and G. R. Irwin, "The stress analysis of cracks handbook," 3rd ed., American Society of Mechanical Engineers, New York, 2000.

[35] R.A. Pitts, S. Carpentier, F. Escourbiac, T. Hirai, V. Komarov, S. Lisgo, A.S. Kukushkin, A. Loarte, M. Merola, A. Sashala Naik, R. Mitteau, M. Sugihara, B. Bazylev, and P.C. Stangeby, "A full tungsten divertor for ITER: Physics issues and design status," *Journal of Nuclear Materials* **438**, S48-S56 (2013).

[36] J. H. Weaver, J. Yang, and F. W. Zok, "Control of interface properties in oxide composites via fugitive coatings," *Journal of the American Ceramic Society* **91**(12), 4003-4008 (2008).

[37] S. Antusch, P. Norajitra, V. Piotter, H.-J. Ritzhaupt-Kleissl, and L. Spatafora, "Powder injection molding – An innovative manufacturing method for He-cooled DEMO divertor components," *Fusion Engineering and Design* **86**, 1575-1578 (2011).

[38] W. J. Clegg, "The fabrication and failure of laminar ceramic composites," *Acta Metallurgica et Materialia* **40**(11), 3085-93 (1992).

Appendix

Experimental Data

W wire tensile testing: engineering stress vs. normalized displacement

15-μm wire

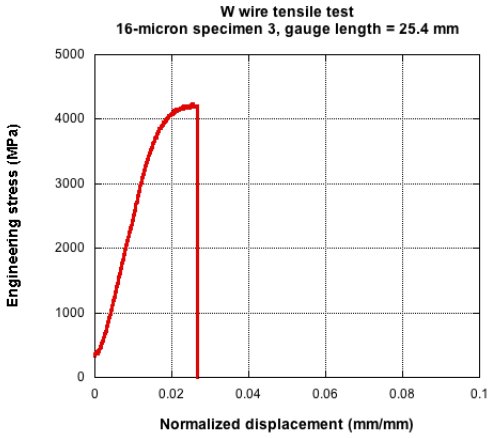

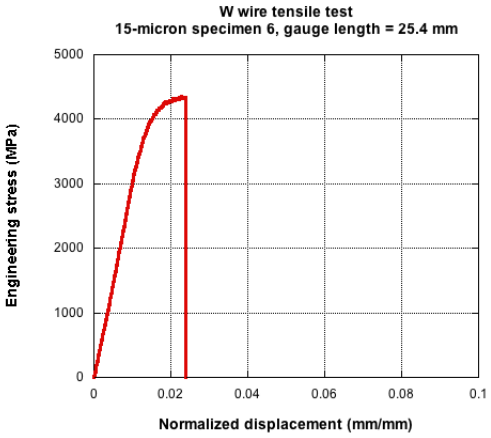

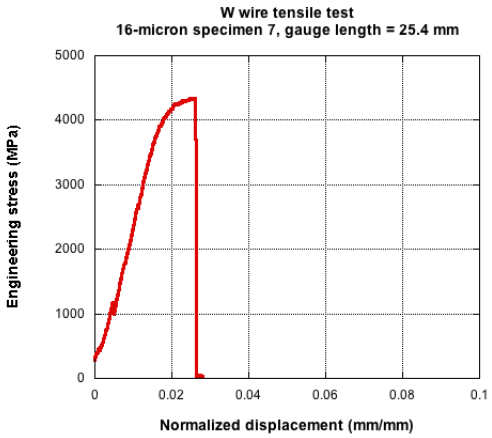

W wire tensile testing: engineering stress vs. normalized displacement

250-µm wire

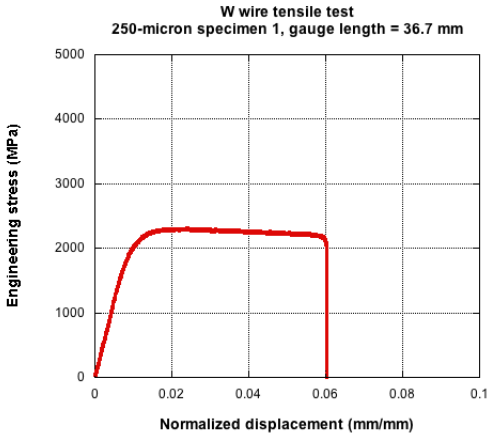

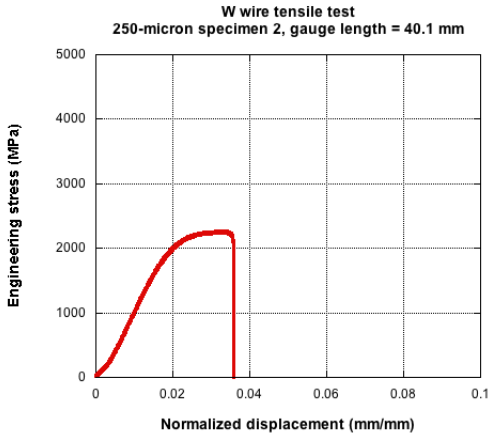

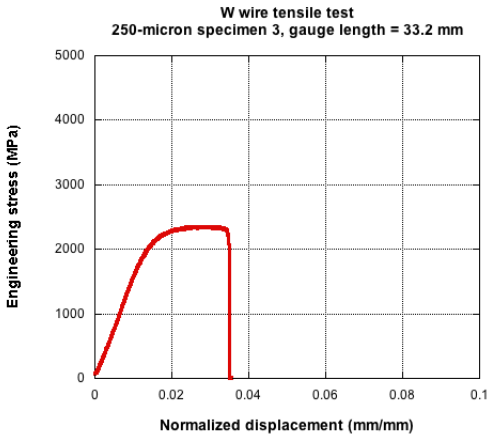

W wire tensile testing: engineering stress vs. normalized displacement

500-μm wire

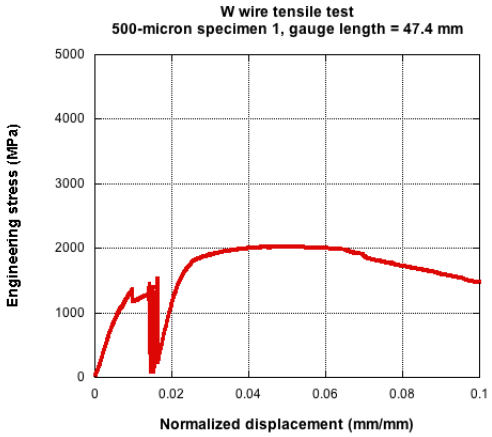

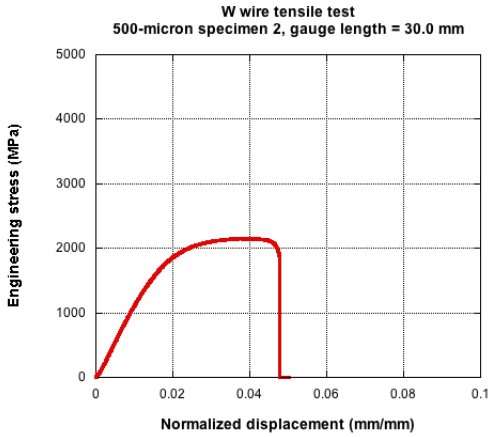

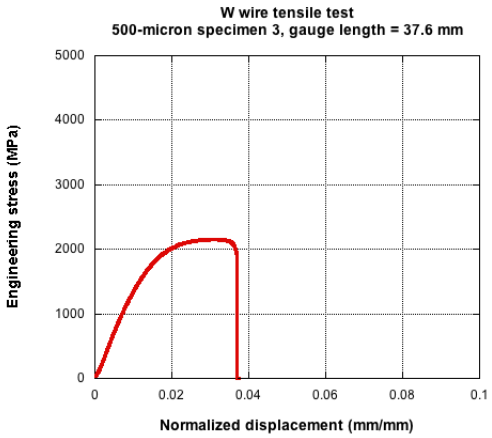

EBSD grain maps and pole figures for W wire

As-received W wire

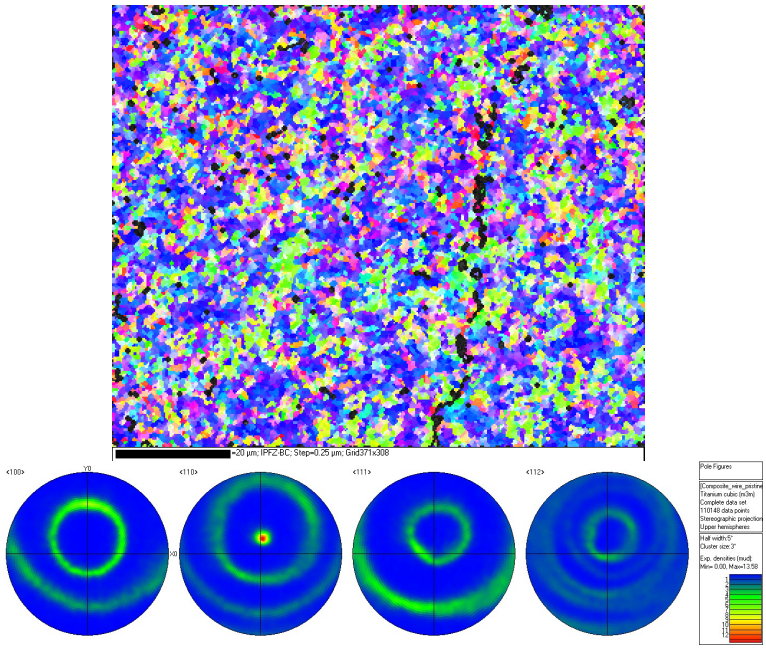

Post-processing W wire
(Upper right: sintered W matrix;
pole figures from wire area only)

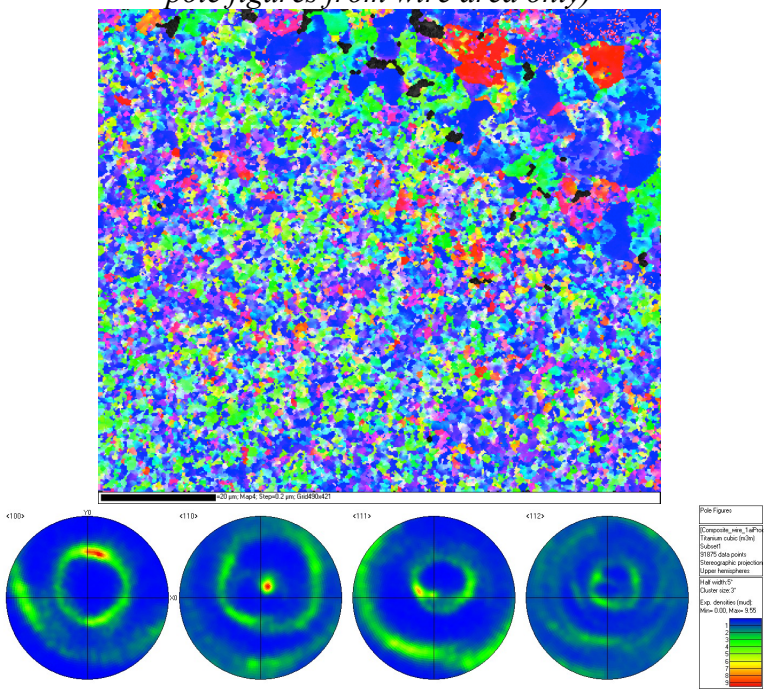

W and Cu foil tensile testing: engineering stress vs. engineering strain

W foil

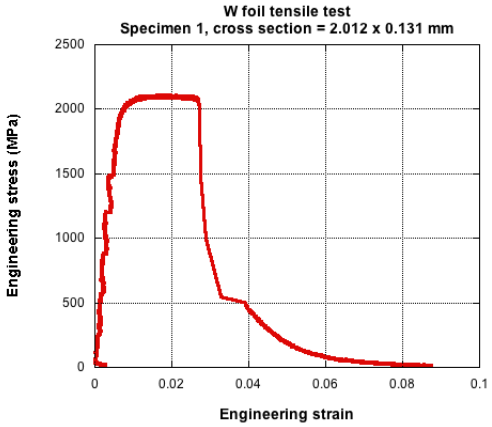

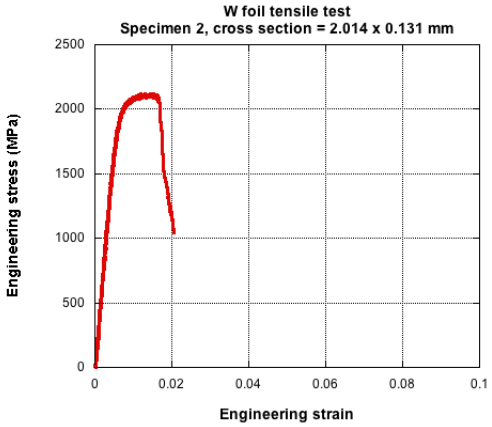

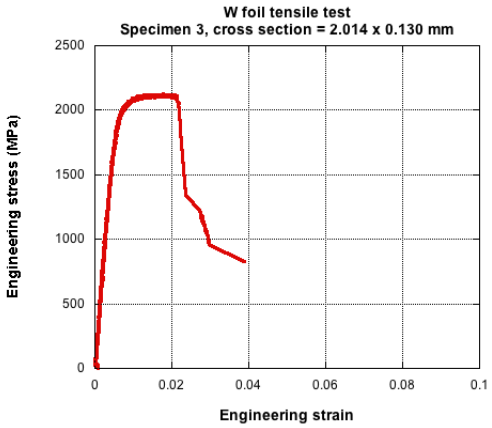

Cu foil

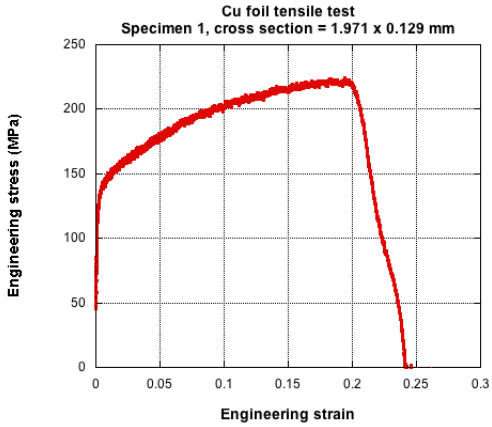

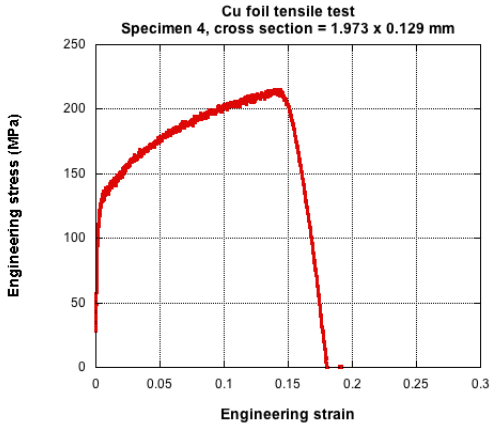

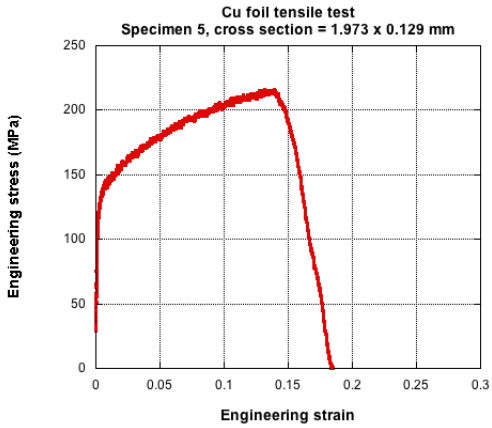

W plate fracture toughness testing: load vs. crosshead displacement

L orientation

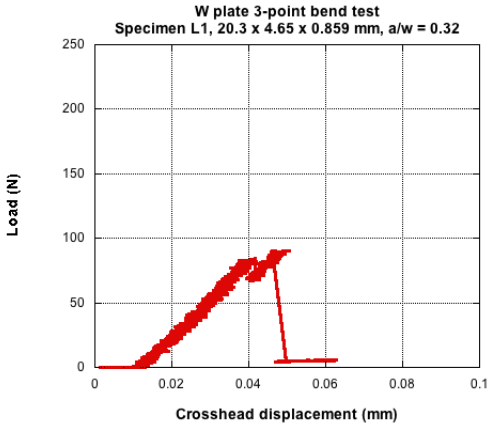

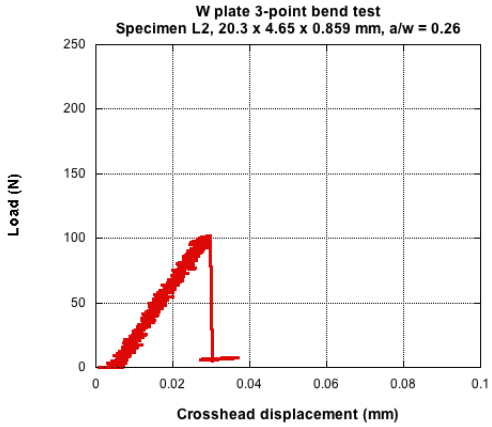

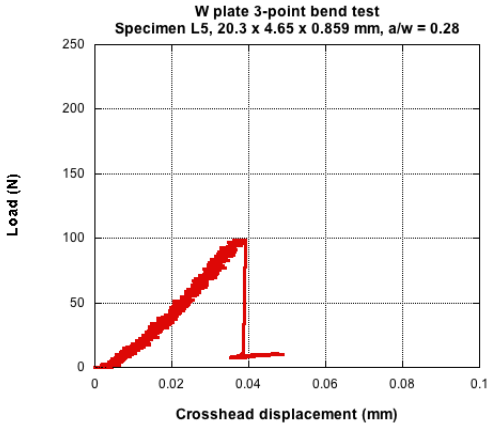

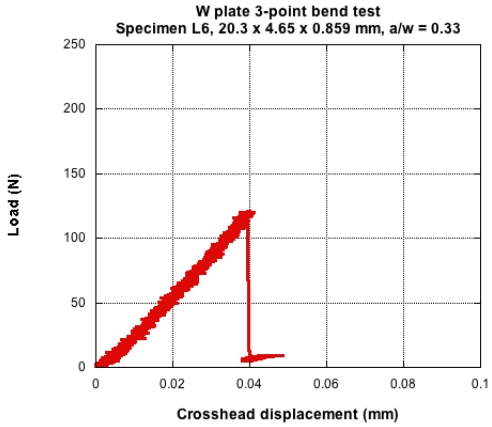

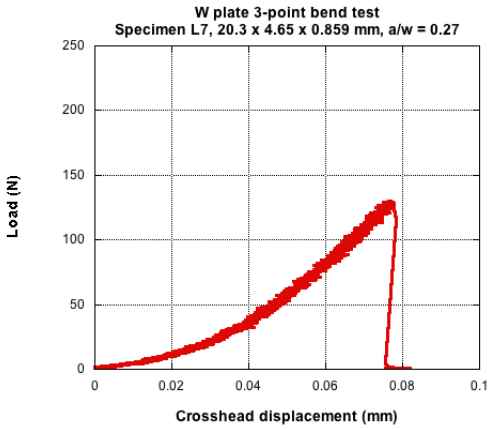

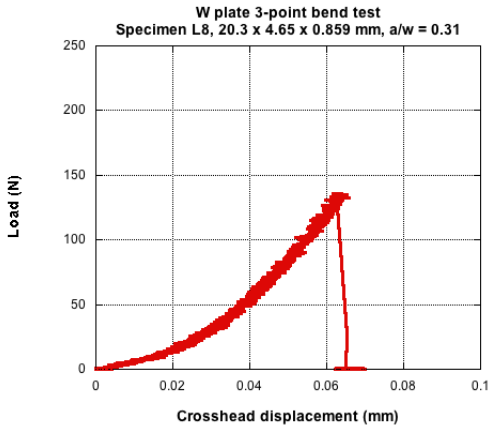

W plate fracture toughness testing: load vs. crosshead displacement

T orientation

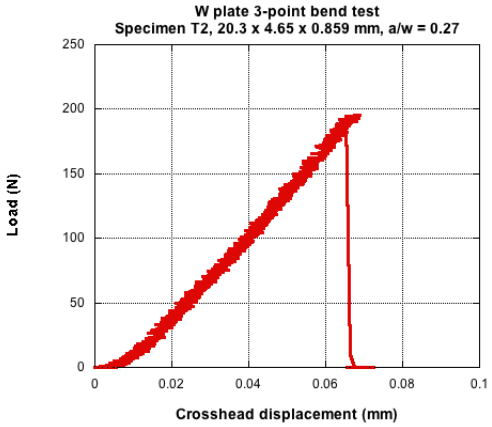

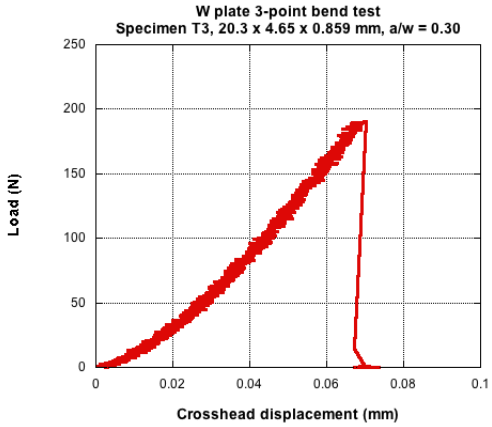

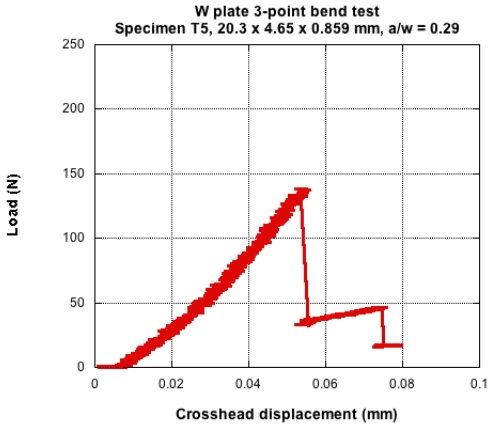

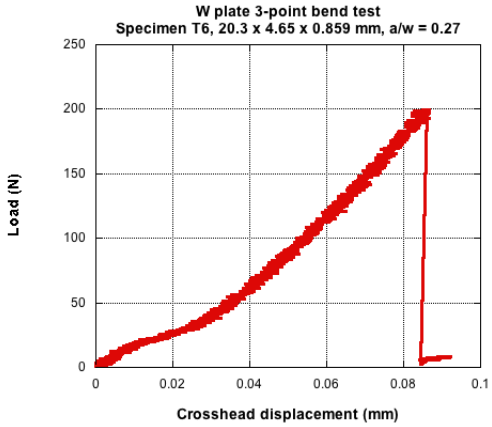

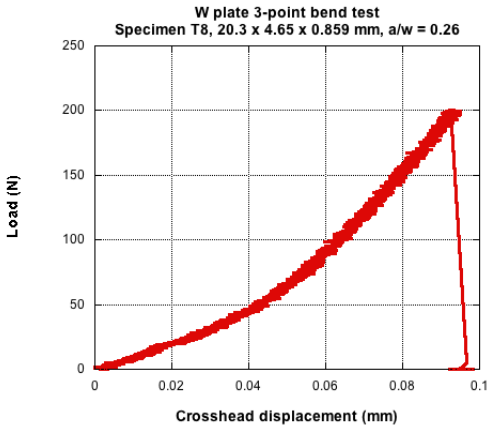

W-WC sintered composite 3-point bend testing: load vs. crosshead displacement

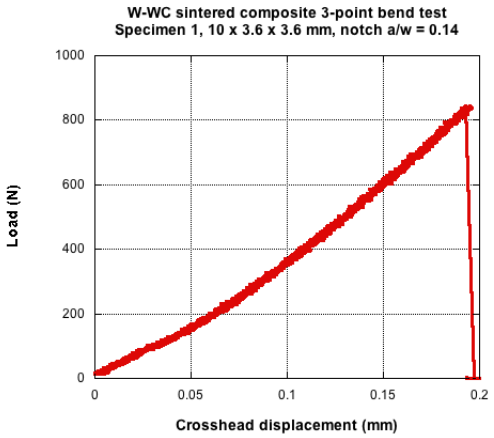

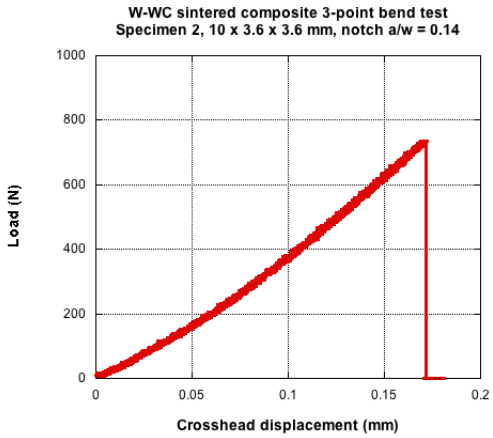

W-Cu hot-pressed laminate testing

Reinforcement tensile testing: engineering stress vs. crosshead displacement

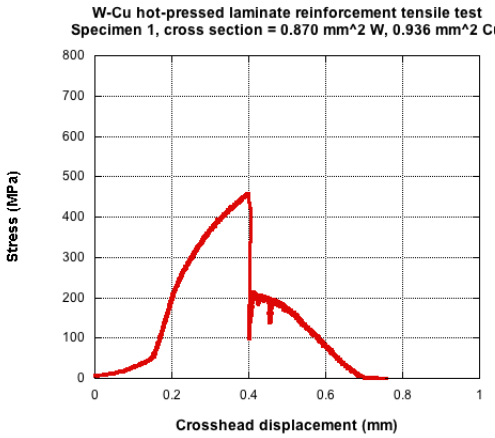

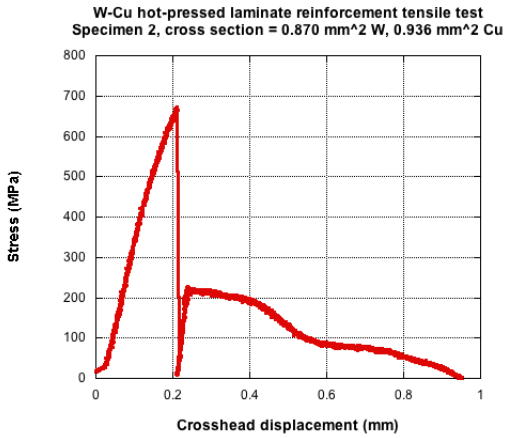

Laminate 3-point bend testing: load vs. crosshead displacement

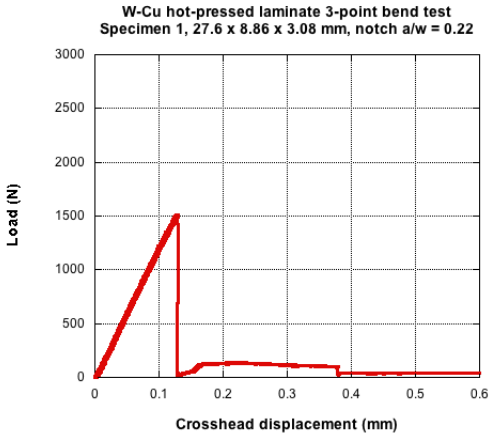

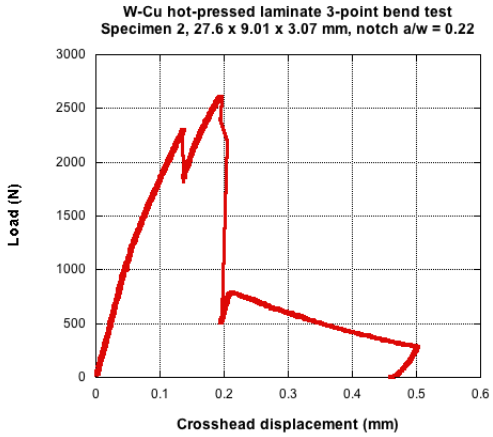

W-Cu brazed laminate: P-D curves and R-curves

L orientation specimens

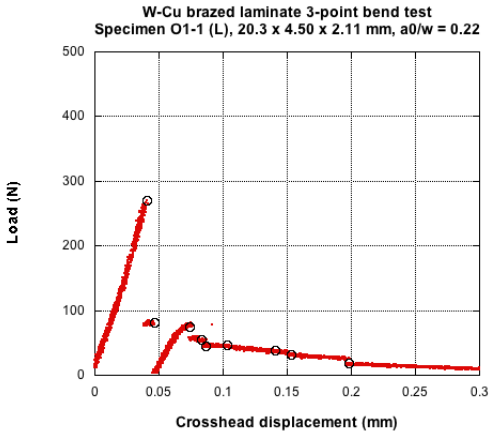

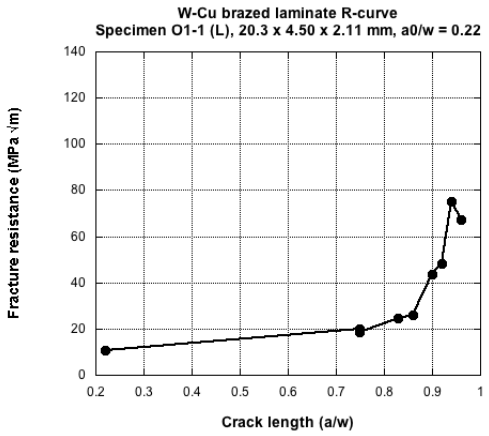

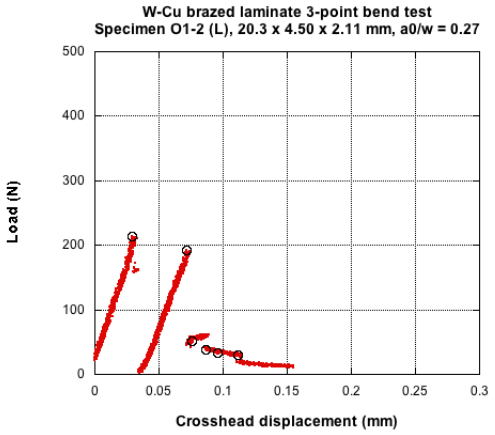

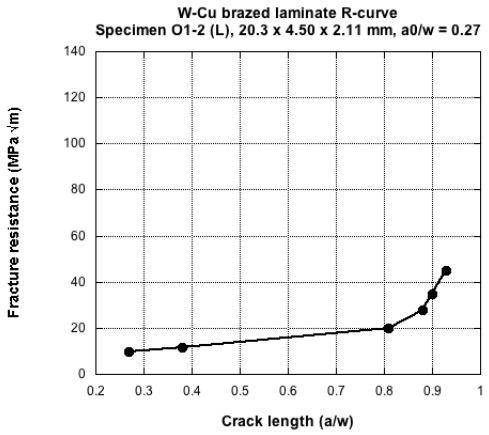

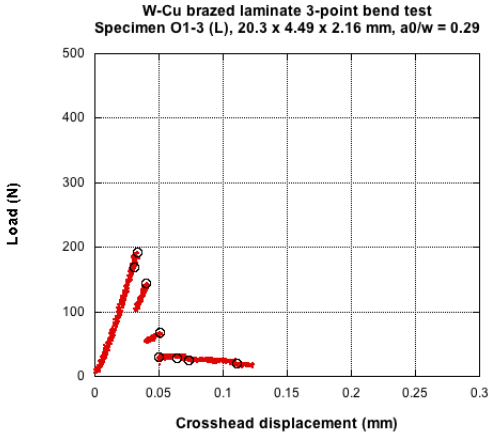

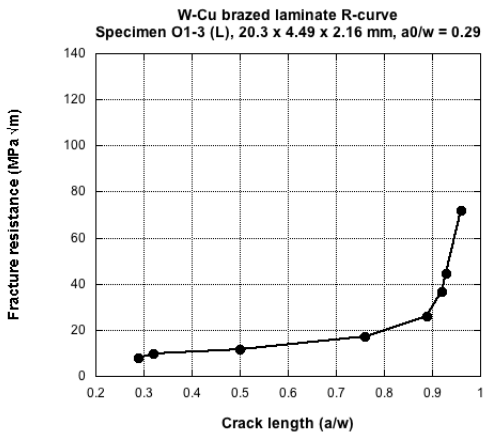

W-Cu brazed laminate: P-D curves and R-curves

T orientation specimens

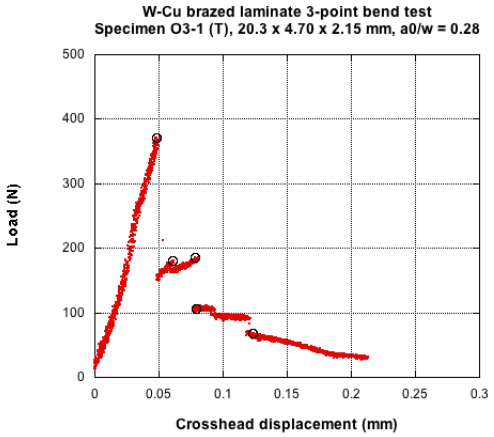

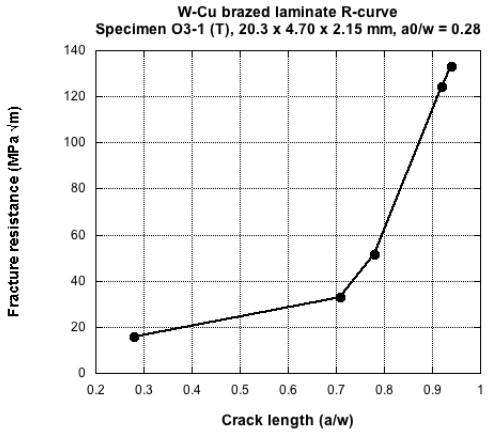

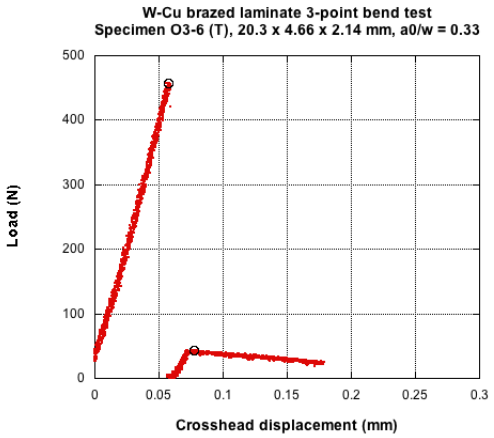

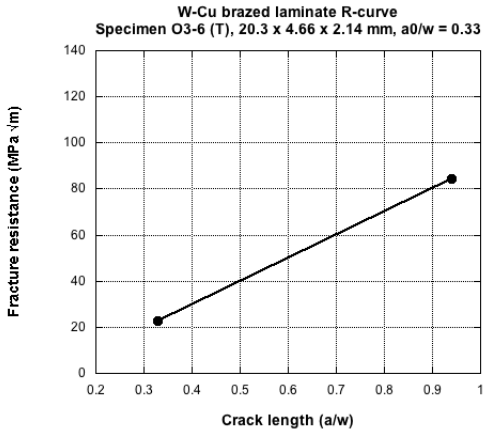

W-Cu brazed laminate: P-D curves and R-curves

Mixed orientation specimens

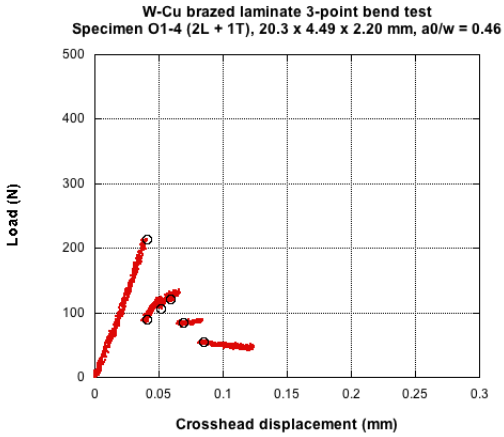

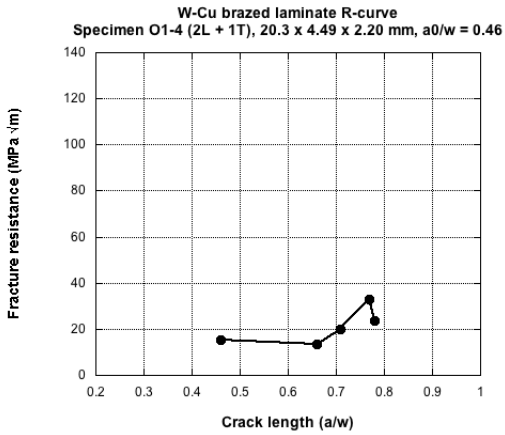

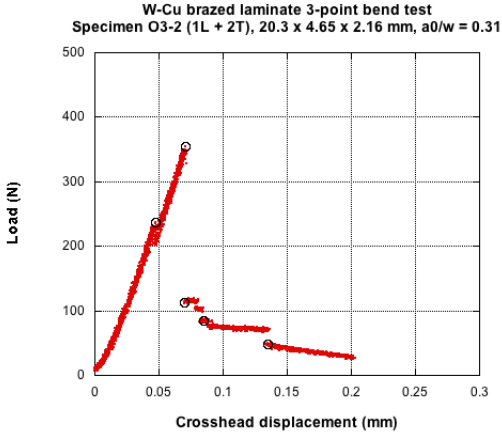

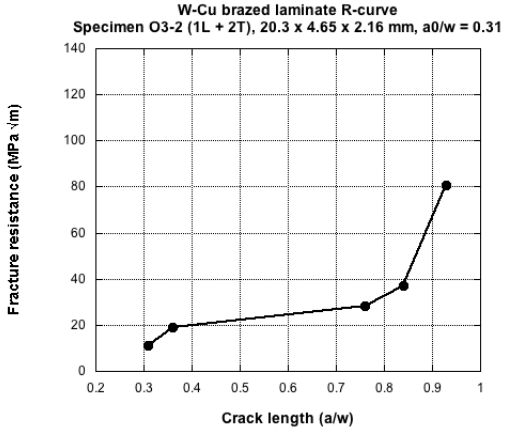

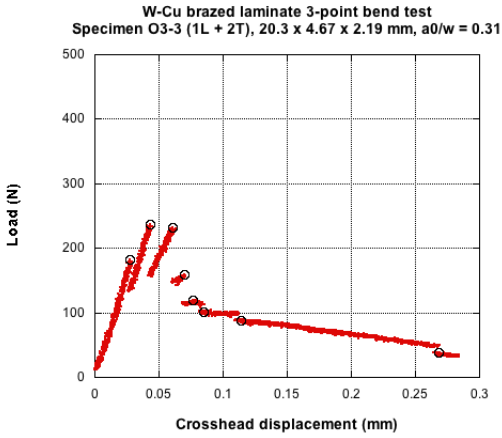

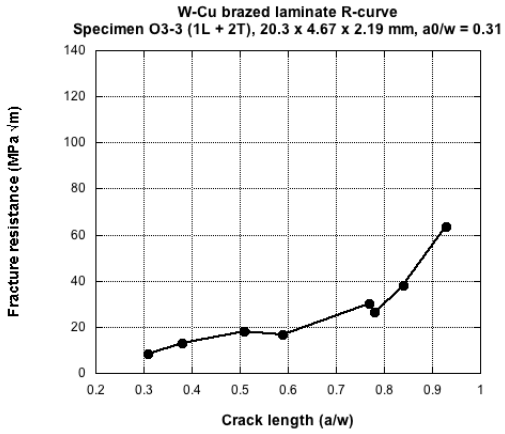

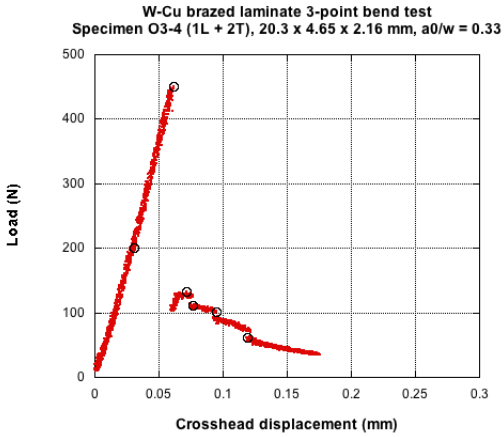
W-Cu brazed laminate 3-point bend test
Specimen O3-4 (1L + 2T), 20.3 x 4.65 x 2.16 mm, a0/w = 0.33
Load (N)
Crosshead displacement (mm)

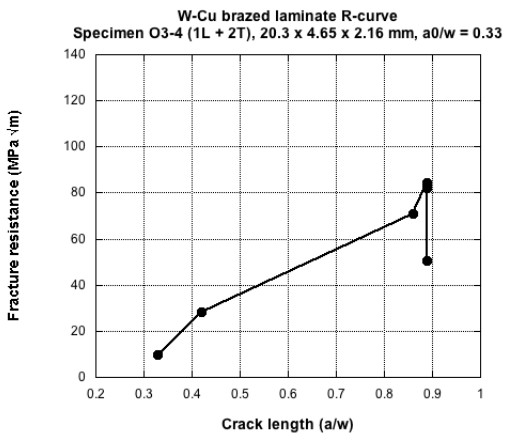
W-Cu brazed laminate R-curve
Specimen O3-4 (1L + 2T), 20.3 x 4.65 x 2.16 mm, a0/w = 0.33
Fracture resistance (MPa √m)
Crack length (a/w)

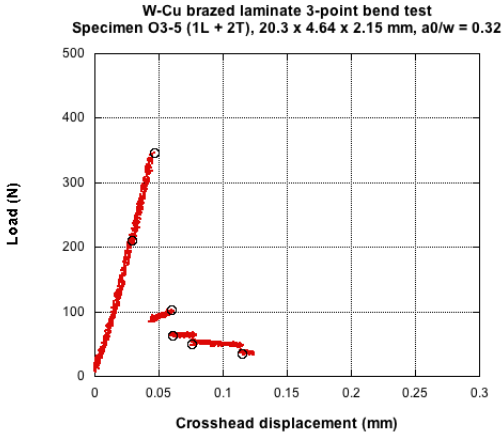
W-Cu brazed laminate 3-point bend test
Specimen O3-5 (1L + 2T), 20.3 x 4.64 x 2.15 mm, a0/w = 0.32
Load (N)
Crosshead displacement (mm)

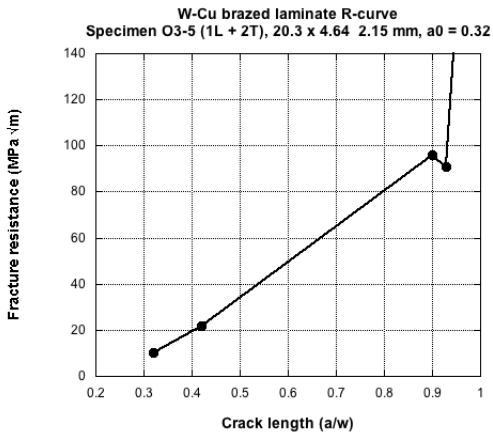
W-Cu brazed laminate R-curve
Specimen O3-5 (1L + 2T), 20.3 x 4.64 2.15 mm, a0 = 0.32
Fracture resistance (MPa √m)
Crack length (a/w)

Large-Scale Crack Bridging Code

Large - Scale Bridging Code: Case 1

```
ClearAll["Global`*"];
```

Input data

Specimen Geometry

```
w = 0.01524; (* width in m *)
s = 4 w; (* span in m *)
b = 0.00508; (* thickness in m *)
a0 = 0.41 w ; (* Pre-crack depth in m *)
shape[x_] := 1 (*Face orientation meshing shape function*)
```

Matrix properties

```
e = 172 (10^9); (* Young's modulus in Pa *)
v = 0.33; (* Poisson's ratio *)
KIC = 8 (10^6); (* matrix toughness in Pa√m*)
```

Bridging law parameters

```
σmax = 200 (10^6); (* peak stress in Pa *)
Δ1 = 2 (10^-6); (* displacement at peak stress in m *)
Δ2 = 110 (10^-6); (* failure displacement of bridging ligaments in m *)
n = 1; (* post-peak shape parameter *)
σr = 0; (* residual stress in ductile phase *)
```

Calculation parameters

```
inc = 0.05 w; (* crack growth increment in m *)
conv = 1; (* convergence criterion for stress distribution in Pa *)
cconv = 0.0001; (* convergence criterion for bridging zone length as a fractional change *)
breakcheck = 0.9999; (*convergence criterion to resolve instances where the error in stress distribution oscillates*)
maxbreak = 5; (*maximum number of times the error can increase with each iteration in the stress disctribution calculation;
lower values may cause convergence on local minima insteaed of global minumum*)
```

Calculation

List Setup

```
a1 = a0 + inc; (* first calculated crack length *)
c = a0; (* set the initial bridging zone edge as the precrack length *)
a = a1; (* set the first crack growth increment for calculating K_TR *)
ee = e / (1 - v^2); (* Plane strain Young's modulus *)
gg = e / (2 + 2 v); (* Shear modulus *)
σguess = σmax; (* guess for crack face traction in Pa *)
ninc = Round[(w - a0) / inc];

(* Creates lists that will be filled during iteration, starting from initial values *)
alist = {a0}; (*list of all crack lengths used to calculate the R-curve*)
clist = {a0}; (*list for values of the end of the bridging zone calculated for each crack length*)
Klist = {KIC}; (*list of K_TR values*)
plist = {0}; (*list of applied loads*)
dlist = {0}; (*list of load-point displacements*)
error = {0}; (*list of the convergent error for the stress distribution for each crack length*)
finalerrordist = {}; (*list of the distribution of bridging-stress errors along the crack face for each crack length*)
finalstressevolution = {}; (*list of the stress distributions for each crack length*)
finalcrackevolution = {}; (*list of the crack shapes for each crack length*)
finalopeningevolution = {}; (*list of crack opening displacement distributions*)
finalclosingevolution = {}; (*list of crack closing displacement distributions*)
points = {0}; (*number of points in the mesh for each crack length*)
```

Function Definitions

```
(* Bridging law *)
σb[u_] := Piecewise[{{0, u < 0}, {(σmax - σr) (u / Δ1), 0 ≤ u ≤ Δ1}, {(σmax / 2) (1 - (u - Δ1) / (Δ2 - Δ1)) ^ n + (σmax / 2) (1 - ((u - Δ1) / (Δ2 - Δ1)) ^ (1 / n)), Δ1 < u ≤ Δ2},
    {0, Δ2 < u}}];

(* Correction factor for 3pb K_{I,P}*)
F1[x_] := Pi ^ -0.5 (1.99 - x (1 - x) (2.15 - 3.93 x + 2.7 x ^ 2)) / ((1 + 2 x) (1 - x) ^ 1.5);

(*Correction factor for 3pb K_{I,P};*)
g1[x_] := 0.46 + 3.06 x + 0.84 (1 - x) ^ 5 + 0.66 x ^ 2 (1 - x) ^ 2;
g2[x_] := -3.52 x ^ 2;
g3[x_] := 6.17 - 28.22 x + 34.54 x ^ 2 - 14.39 x ^ 3 - (1 - x) ^ 1.5 - 5.88 (1 - x) ^ 5 - 2.64 x ^ 2 (1 - x) ^ 2;
g4[x_] := -6.63 + 25.16 x - 31.04 x ^ 2 + 14.41 x ^ 3 + 2 (1 - x) ^ 1.5 + 5.04 (1 - x) ^ 5 + 1.98 x ^ 2 (1 - x) ^ 2;
G[x_, y_] := g1[y] + g2[y] x + g3[y] x ^ 2 + g4[y] x ^ 3;
F2[x_, y_] := G[x, y] / (1 - (y)) ^ 1.5 / (1 - (x) ^ 2) ^ 0.5;

(* Stress intensity at crack tip due to a pair of point forces on the crack face *)
KIF[f_, x_, a_] := 2 f / (Pi a) ^ 0.5 F2[x / a, a / w];

(* Stress intensity at the crack tip due to remote loading in 3-point bending *)
KIP[P_, a_] := (6 / w ^ 2) (P s / 4) (Pi a) ^ 0.5 F1[a / w]; (*P (Pi a)^0.5 F3[a/w];*)

(*Crack opening displacements from remote loading*)
ΔP[z_] := 2 / ee NIntegrate[KIP[Pguess, x] D[KIF[f, z, x], f], {x, z, a}, Method → {Automatic, "SymbolicProcessing" → 0}, MaxRecursion → 0];

(*Crack closing displacements from bridging - requires nested numerical integration*)
ΔFinner[z_?NumericQ, a_?NumericQ] := NIntegrate[KIF[σx[aaa], aaa, a], {aaa, c, z}, Method → {Automatic, "SymbolicProcessing" → 0}, MaxRecursion → 0];

ΔF[z_, zz_] := 2 / ee NIntegrate[ΔFinner[aa, aa] D[KIF[f, z, aa], f], {aa, zz, a}, Method → {Automatic, "SymbolicProcessing" → 0}, MaxRecursion → 0];

(*Remote load (3pb) for specified crack length and applied stress intensity*)
P[KI_, a_] := KI / (6 s / (4 w ^ 2) (Pi a) ^ 0.5 F1[a / w]);

(*Function used in calculation of load-point displacements*)
V2[x_] := (x / (1 - x)) ^ 2 (5.58 - 19.57 x + 36.82 x ^ 2 - 34.94 x ^ 3 + 12.77 x ^ 4);

(*Initial guess for bridging zone stress distribution*)
σx = Interpolation[{{-20 ^ -10, 0}, {c - 10 ^ -10, 0}, {c, σguess}, {a, σguess}, {a + 10 ^ -10, 0}, {w, 0}}, InterpolationOrder → 1];

(*Face orientation meshing shape function*)
shape[x_] := 1
```

Iterative Calculation

```
(*Iterator to keep track of which crack increment is being calculated*)
loop = 0;

(*Output useful information about the state of the calculation*)
Print["Crack length (a/w), increments remaining, and error"]
Dynamic[{a / w, loop - ninc, esum}]

While[a < w,

  loop++; (*keep track of iteration number*)

  Label["resetc"]; (*if the bridging zone size is changing, the calculation will restart from here*)

  (*Ratios for scaling the distribution of guess points when the bridging zone changes size*)
  If[loop == 1, (*If this loop is removed, the mesh will have the same density for each crack length;
   otherwise the same number of points will be used for each iteration. The non-
    adaptive strategy has not shown significant error in tests of the code, and it significantly reduces computation time. *)
   scale1 = (a - c) / (a1 - a0);
   scale2 = c / a0;

   (*These values can be adjusted: higher numbers mean a denser mesh and longer calculation time*)
   xxx1 = Round[10 scale2]; (*mesh density in the short region near crack mouth*)
   xxx2 = Round[10 scale2]; (*mesh density for the majority of the non-bridged portion of the crack*)
   xxx3 = Round[10 scale2]; (*mesh density in the non-bridged region near the edge of the bridging zone*)
   xxx4 = Round[40 scale1]; (*mesh density in the short region in the bridging zone near its edge*)
   xxx5 = Round[15 scale1]; (*mesh density for the majority of the bridging zone*)
   xxx6 = Round[40 scale1]; (*mesh density near the crack tip*)

   (*Define the mesh of x-values at which the crack face displacements and stresses will be calculated*)
   cdata = Join[Array[# * 0.03 / xxx1 &, xxx1 + 1, 0], Array[0.03 + # * (0.96 - 0.03) / xxx2 &, xxx2, 1], Array[0.96 + # * (1 - 0.96) / xxx3 &, xxx3 - 1, 1]];

   bridgex = Join[Array[# * 0.25 / xxx4 &, xxx4, 1], Array[0.25 + # (0.75 - 0.25) / xxx5 &, xxx5, 1], Array[0.75 + # (1 - 0.75) / xxx6 &, xxx6, 1]]
  ];

  (*mesh of points for calculating stress distribution and crack-face displacements*)
  guessx = Sort[Join[cdata c, {c - 10 ^ -10, c, c + 10 ^ -10}, c + bridgex (a - c)]];

  (*Set an initial value for the error in the stress distribution and create an empty list for the series of error values*)
  esum = 1 000 000 000. ee; (*an arbitrarily high initial guess value that will be higher than the convergence criterion *)
  elist = {esum}; (*a list that will hold the error in the stress distribution and allow for convergence checks*)

  (*Create lists for the internal iteration process, where the lowest-error solution will be put into the main solution list*)
  stressevolution = {}; (*holds the stress distribution list as it converges; the convergent value is saved in the list defined above*)
  crackevolution = {}; (*same function, for crack shape*)
  closingevolution = {}; (*same function, for closing displacements*)
  openingevolution = {}; (*same function, for opening displacements*)
  Klist1 = {}; (*same function, for K_TIP*)
  plist1 = {}; (*same function, for P*)
  error1 = {}; (*same function, for error in stress distribution*)
  errordist = {}; (*same function, for distribution of errors on crack face*)

  break = 0; (*initial value for a counter that allows a certain number of increases in error to occur,
  in an attempt to move past local minima towards the global minimum*)
```

```
(* Iterative loop that calculates opening profile and stresses using stress distribution convergence criterion *)
While[ϵsum > conv,

 (*A check to make sure that the mesh of x-values does not force the code to attempt to make any calculations beyond the crack tip*)
 While[guessx[[Length[guessx]]] > a, guessx = Delete[guessx, -1]];

 (*Calculate the total stress intensity reduction due to the bridging zone, the applied stress intensity, and applied load*)
 Clear[ΔKIF, KIR, Pguess];
 ΔKIF = NIntegrate[KIF[ shape[aaa] σx[aaa], aaa, a], {aaa, c, a}, Method → {Automatic, "SymbolicProcessing" → None}, MaxRecursion → 0];
 (*calculated stress intensity shielding due to bridging zone;
 integrals are optimized for speed and errors are reduced by multiple iterative passes*)
 KIR = KIC + ΔKIF; (*calculated fracture resistance*)
 Pguess = P[KIR, a]; (*calculated applied load*)

 (*Calculate the constant value for crack face closing displacements at all points behind the bridging zone*)
 Clear[opening, closing, Δnet, σdist];

 (*Calculate crack face opening displacements at all mesh points*)
 opening = Array[If[guessx[[#]] ≥ a, 0, Re[ΔP[guessx[[#]]]], 10^-10] &, Length[guessx]];

 (*Calculate crack face closing displacements at all mesh points*)
 (*using this loop structure prevents memory overflow*)
 counter1 = 1;
 closing = Re[Reap[
       Do[
        Sow[
         If[guessx[[counter1]] ≤ c,
          ΔF[guessx[[counter1]], c],
          ΔF[guessx[[counter1]], guessx[[counter1]]]
         ]
        ];
        ++counter1;
        , {Length[guessx]}
       ]
      ]
      [[2]]
     [[1]]
 ];

 (*Calculate net crack face displacements, preventing negative values*)
 Δnet = Array[If[opening[[#]] - closing[[#]] < 0, 0, opening[[#]] - closing[[#]]] &, Length[guessx]];

 (*Calculate crack face stresses at all mesh points using bridging law*)
 σdist =  Array[ Re[σb[Δnet[[#]]]] &, Length[guessx]];

 (*Ensure that there is no stress behind the bridging zone; broken ligaments are handled by the definition of σdist*)
 Do[σdist = Delete[σdist, 1]
  , {Length[Select[guessx, # < c &]]}];
 Do[PrependTo[σdist, 0]
  , {Length[Select[guessx, # < c &]]}];

 (*Make sure there are no undefined points in the functions over the entire width of the specimen by adding the values of each distribution at x=
  w*)
 AppendTo[guessx, w];
 AppendTo[σdist, 0];
 AppendTo[Δnet, 0];
 AppendTo[closing, 0];
 AppendTo[opening, 0];

 (*Interpolate over the stress distribution*)
 Clear[σinterp];
 σinterp = Interpolation[Transpose@{guessx, σdist}, InterpolationOrder → 1];

 (*Calculate the error in stress at each mesh point and sum absolute values for a total error*)
 ϵx = σdist - Array[ Re[shape[guessx[[#]]] σx[guessx[[#]]]] &, Length[guessx]];
 ϵsum = Sum[Abs[ϵx[[x]]], {x, Length[ϵx]}];

 (*Safety checks to prevent infinite looping*)
 check = (Min[ϵlist] - ϵsum) / Min[ϵlist];
 If[check ≤ 0, ++break];
 If[break > maxbreak, Break[]];
 If[break > 0, If[Abs[check] > breakcheck, Break[]]];

 (*Record the calculated values for this intermediate iteration to allow for examination of how the distribution converges to a self-
  consistent solution*)
 AppendTo[stressevolution, Transpose@{guessx, σdist}];
 AppendTo[crackevolution, Transpose@{guessx, Δnet}];
 AppendTo[openingevolution, Transpose@{guessx, opening}];
 AppendTo[closingevolution, Transpose@{guessx, closing}];
 AppendTo[Klist1, KIR];
 AppendTo[plist1, Pguess];
 AppendTo[error1, ϵsum];
 AppendTo[errordist, Transpose@{guessx, ϵx}];
 AppendTo[ϵlist, ϵsum];

 Clear[σx];
 (*update the stress distribution for the next iteration*)
 σx = σinterp;

 (*stop if any of the stress distributions in the list are identical*)
 If[Min[ϵlist] == 0, Break[]];

];
```

```
  cguess = c; (*save the current end of the bridging zone for comparison*)

  result = Extract[Position[error1, Min[error1]] , {1, 1}]; (*make sure that the lowest-error solution is recorded later on*)

  Clear[crackshape, ccheck];

  crackshape = Interpolation[crackevolution[[result]], InterpolationOrder → 1]; (*define a continuous function for the crack shape*)

  ccheck = If[Max[Transpose[crackevolution[[result]]][[2]]] ≥ Δ2, x /. FindRoot[crackshape[x] == Δ2, {x, a0 / 2}], 0];
  (*define the point in the crack shape that reaches the failure displacement of the reinforcement*)

  c = Max[ccheck, a0]; (*update the bridging zone length*)

  If[Abs[(c - cguess) / cguess] ≥ cconv, Goto["resetc"]]; (*check convergence criterion for brisging zone length*)

  (*Record convergent solutions for this crack length*)
  AppendTo[alist, a];
  AppendTo[clist, c];
  AppendTo[Klist, Klist1[[result]]];
  AppendTo[plist, plist1[[result]]];
  AppendTo[error, error1[[result]]];
  AppendTo[finalstressevolution, stressevolution[[result]] ];
  AppendTo[finalcrackevolution, crackevolution[[result]] ];
  AppendTo[finalopeningevolution, openingevolution[[result]] ];
  AppendTo[finalclosingevolution, closingevolution[[result]] ];
  AppendTo[finalerrordist, errordist[[result]]];
  AppendTo[points, Length[guessx]];

  (* Increase crack length and increase counter for loop *)
  a += inc;
 ];

(* Calculate load-displacement curve *)
qq = 1;
Do[
  ++qq;
  Clear[σx];
  σx = Interpolation[finalstressevolution[[qq - 1]], InterpolationOrder → 1];
  Δnc = plist[[qq]] (s^3 / (4 ee w^3) + s / (2 w) (3 / (4 gg) - 3 / (10 ee) - 3 ν / (4 ee)) - 0.21 / ee);
  Δc = 6 plist[[qq]] s^2 / (4 ee w^2) V2[alist[[qq]] / w];
  Δbrinner[x_?NumericQ] := NIntegrate[KIF[σx[xx], xx, z], {xx, clist[[qq]], z}, Method → {Automatic, "SymbolicProcessing" → None}];
  Δbr = Re[2 / ee NIntegrate[Δbrinner[x] D[KIF[P, x], P], {x, clist[[qq]], alist[[qq]]}, Method → {Automatic, "SymbolicProcessing" → None}]];
  d = (Δc + Δnc) - Δbr;
  AppendTo[dlist, d];
  , {Length[plist] - 1}];

(*Set crack length to the final value*)
a = alist[[Length[alist]]];
```

Solution Output

```
(*Output a table of values from the calculation*)
data = Transpose[{Round[alist * 1000, 0.01], Round[alist / w, 0.01], Klist / 1 000 000, Round[plist b, 0.01], Round[dlist * 1000, 0.001],
    Round[(alist - clist) * 1000, 0.001], Round[error / 1 000 000, 0.001], points}];
PrependTo[data, {"mm", "-", "MPa" Superscript["m", "0.5"], "N", "mm", "mm", "MPa", "#"}];
PrependTo[data, {"a", "a/w", "K_IR", "P", "D", "LSB size", "Error-σ", "Points"}];
Grid[data, Frame → All]

(*Plot the bridging law*)
Plot[σb[u] , {u, 0, Δ2}, PlotLabel → "Bridging Law", AxesLabel → {"Displacement (m)", "Stress (Pa)"}, PlotStyle -> Thickness[Large],
 PlotRange → {{0, 1.2 Δ2}, {0, σmax}}]

Clear[rcurve, loaddisp];

(*Plot the resistance curve*)
rcurve = Transpose@{(alist) / w, Klist / 1 000 000};
ListLinePlot[rcurve, PlotRange → {{a0 / w, 1}, {0, Max[Klist] / 1 000 000}}, Epilog → Point[rcurve], PlotLabel → "Resistance curve",
 AxesLabel → {"Crack extension (m)", "Fracture resistance (Pa m^0.5)"}, AxesOrigin → {a0 / w, 0}, PlotStyle -> {{Thick, Blue}}]

(*Load-displacement curve is normalized by values for unbridged specimen*)
pp = P[KIC, a0]; (*calculate pure-matrix failure load*)
Δnc = pp (s^3 / (4 ee w^3) + s / (2 w) (3 / (4 gg) - 3 / (10 ee) - 3 ν / (4 ee)) - 0.21 / ee);
Δc = 6 pp s^2 / (4 ee w^2) V2[a0 / w];
dd = Δc + Δnc; (*calculate pure-matrix failure displacement*)
loaddisp = Transpose@{dlist / dd, plist / pp};
ListLinePlot[loaddisp, PlotRange → {{0, Max[dlist] / dd}, {0, Max[plist] / pp}}, Epilog → Point[loaddisp], PlotLabel → "Load-displacement curve",
 AxesLabel → {"Load-point displacement (m)", "Load (N)"}, PlotStyle → {{Thick, Blue}, {Thick, Black, Dashed}}]

(*Plot the evolution of the crack shape over the entire specimen*)
(*grid lines show location of precrack and the failure displacement of the reinforcement*)
Show[Array[ListLinePlot[finalcrackevolution[[#]], PlotRange → All, PlotStyle -> Thickness[Large]] &, Length[finalcrackevolution]],
 PlotRange → {{0, w}, {0, Max[finalcrackevolution[[All, All, 2]]]}}, GridLines → {{a0}, {Δ2}}, PlotRangePadding → None, AxesOrigin → {0, 0},
 PlotLabel → "Crack growth evolution", AxesLabel → {"Position (m)", "Crack opening (m)"}]

(*Plot the crack shape only for the bridging zone, from the precrack to w*)
Show[Array[ListPlot[finalcrackevolution[[#]], PlotRange → All, PlotStyle -> Thickness[Large]] &, Length[finalcrackevolution]],
 PlotRange → {{a0, w}, {0, Δ2}}, PlotRangePadding → None, AxesOrigin → {a0, 0}, PlotLabel → "Crack growth evolution (Bridging zone only)",
 AxesLabel → {"Position (m)", "Crack opening (m)"}]

(*Plot the opening displacements used in the calculation*)
Show[Array[ListPlot[finalopeningevolution[[#]], PlotRange → All, PlotStyle -> Thickness[Large]] &, Length[finalopeningevolution]],
 PlotRange → {{0, w}, {0, Max[finalopeningevolution[[All, All, 2]]]}}, PlotRangePadding → None, AxesOrigin → {0, 0},
 PlotLabel → "Opening displacements only", AxesLabel → {"Position (m)", "Displacement (m)"}]

(*Plot the closing displacements used in the calculation*)
Show[Array[ListPlot[finalclosingevolution[[#]], PlotRange → All, PlotStyle -> Thickness[Large]] &, Length[finalclosingevolution]],
 PlotRange → {{0, w}, {0, Max[finalclosingevolution[[All, All, 2]]]}}, PlotRangePadding → None, AxesOrigin → {0, 0},
 PlotLabel → "Closing displacements only", AxesLabel → {"Position (m)", "Displacement (m)"}]
```

```
(*Plot the evolution of the stress distribution on the crack face with overlaid error bars*)
Needs["ErrorBarPlots`"]
Show[
 Array[
  ErrorListPlot[Transpose[{Transpose[finalstressevolution[[#]]][[1]], Transpose[finalstressevolution[[#]]][[2]],
      Abs[Transpose[finalerrordist[[#]]][[2]]]}],
    ErrorBarFunction → Function[{coords, errs}, {Opacity[1, Red], Line[{coords - {0, errs[[2, 1]]}, coords + {0, errs[[2, 1]]}}]}] &,
  Length[finalstressevolution]], Array[ListLinePlot[finalstressevolution[[#]] &, Length[finalstressevolution]], PlotRange → {{a0, w}, {0, σmax}},
 PlotRangePadding → None, AxesOrigin → {a0, 0}, PlotLabel → "Crack stress distribution", AxesLabel → {"Position(m)", "Stress (Pa)"}]
```

a	a/w	K_{IR}	P	D	LSB size	Error-σ	Points
mm	-	MPa $m^{0.5}$	N	mm	mm	MPa	⌗
6.25	0.41	8	0.	0.	0.	0.	0
7.01	0.46	15.3063	1019.33	0.044	0.762	0.	129
7.77	0.51	21.6935	1237.2	0.059	1.524	0.	129
8.53	0.56	29.1866	1406.1	0.073	2.286	0.	129
9.3	0.61	38.2513	1529.33	0.088	3.048	0.	129
10.06	0.66	50.047	1622.17	0.105	3.81	0.	129
10.82	0.71	65.3083	1662.5	0.124	4.572	0.	129
11.58	0.76	84.3083	1611.76	0.143	5.334	0.	129
12.34	0.81	106.719	1433.22	0.159	6.096	0.	129
13.11	0.86	126.131	1067.39	0.175	6.708	0.	129
13.87	0.91	144.073	624.8	0.214	5.339	0.	129
14.63	0.96	177.653	226.24	0.369	3.329	0.	129

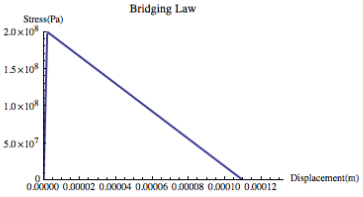

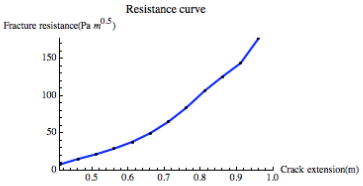

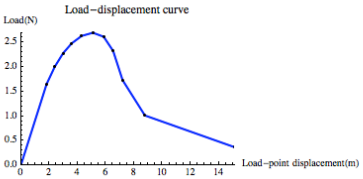

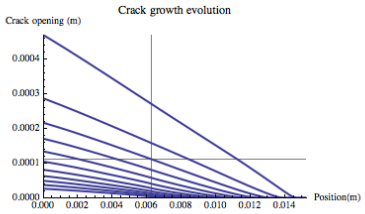

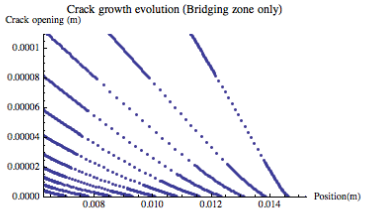

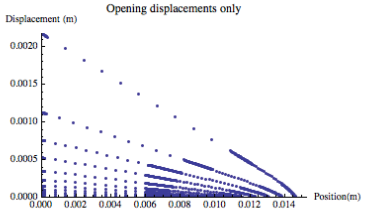

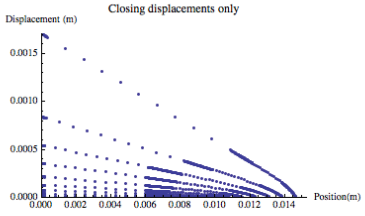

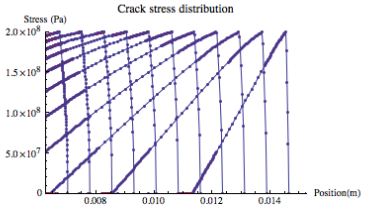

Large - Scale Bridging Code: Case 2

```
ClearAll["Global`*"];
```

Input data

R-Curve and Bridging Law Guess

```
(* Input the R-curve points in lists of a/w and K_IR (MPa) *)
rcurve = Transpose@{{0.5`, 0.52`, 0.54`, 0.56`, 0.58`, 0.6`, 0.65`, 0.7`, 0.75`, 0.8000000000000002`},
    {10.6567122438882`, 13.25389394589456`, 16.340948701249737`, 19.53250502206072`,
     22.906565213184184`, 26.652268761857048`, 38.15539941713198`, 54.45012313651892`,
     80.0983111463113`, 122.29455710376598`}};

rcurveint = Interpolation[rcurve, InterpolationOrder → 1];
```

Bridging Law Guess Values

```
σmax = 1 (10^6); (* peak stress in Pa *)
Δ1 = 0.1 (10^-6); (* displacement at peak stress in m *)
n = 0.0001; (*variable to describe the shape of post-peak curve*)
Δ2 = 350 (10^-6); (* failure displacement of bridging ligaments in m *)
σr = 0; (* residual stress in ductile phase *)
```

Specimen Geometry

```
s = 0.02028698; (* span in m *)
w = s / 4; (* width in m *)
b = w / 2; (* thickness in m *)
shape[x_] := 1; (*Face orientation meshing shape function*)
```

Matrix properties

```
e = 410 (10^9); (* Young's modulus in Pa *)
ν = 0.28; (* Poisson's ratio *)
```

Calculation parameters

```
conv =  0.1*10^6; (* convergence criterion for stress distribution in Pa *)
cconv = 0.0001; (* convergence criterion for bridging zone length as a fractional change *)
breakcheck = 0.9999; (*convergence criterion to resolve instances where the error in stress
 distribution oscillates*)
maxbreak = 5; (*maximum number of times the error can increase with each iteration in the stress
 disctribution calculation; lower values may cause convergence on local minima insteaed of global minumum*)
Δ1step = 0.1*10^-6; (* step size in Δ1 for simultaneous calculation of σmax and Δ1 *)
nconv = 0.01; (*convergence criterion for n as a fractional change*)
npower = 5; (*gain exponent to increase convergence speed for n*)
```

Calculation

List Setup

```
a0 = rcurve[[1, 1]] w ; (* Pre-crack depth in m comes from R-curve*)
a1 = rcurve[[2, 1]] w; (* first calculated crack length comes from R-curve*)
KIC = rcurve[[1, 2]] (10^6); (* matrix toughness comes from R-curve*)

c = a0; (* set the initial bridging zone edge as the precrack length *)
a = a1; (* set the first crack growth increment for calculating K_IR *)
ee = e / (1 - ν^2); (* Plane strain Young's modulus *)
gg = e / (2 + 2 ν); (* Shear modulus *)
σguess = σmax; (* guess for crack face traction in Pa *)
```

```
(* Creates lists that will be filled during iteration, starting from initial values *)
alist = {a0};(*list of all crack lengths used to calculate the R-curve*)
clist = {a0};(*list for values of the end of the bridging zone calculated for each crack length*)
Klist = {KIC};(*list of K_IR values*)
plist = {0};(*list of applied loads*)
dlist = {0};(*list of load-point displacements*)
error = {0};(*list of the convergent error for the stress distribution for each crack length*)
finalerrordist = {};(*list of the distribution of bridging-
 stress errors along the crack face for each crack length*)
finalstressevolution = {};(*list of the stress distributions for each crack length*)
finalcrackevolution = {};(*list of the crack shapes for each crack length*)
finalopeningevolution = {};(*list of crack opening displacement distributions*)
finalclosingevolution = {};(*list of crack closing displacement distributions*)
points = {0};(*number of points in the mesh for each crack length*)

σmaxlist = {};
Δ1list = {};
nlist = {};
```

Function Definitions

```
(* Bridging law *)
σb[Δ_] :=
  Piecewise[{{0, Δ < 0}, {(σmax - σr) (Δ / Δ1), 0 ≤ Δ ≤ Δ1},
    {(σmax / 2) (1 - (Δ - Δ1) / (Δ2 - Δ1)) ^ n + (σmax / 2) (1 - ((Δ - Δ1) / (Δ2 - Δ1)) ^ (1 / n)), Δ1 < Δ ≤ Δ2}, {0, Δ2 < Δ}}];

(* Correction factor for 3pb K_I,P *)
F1[x_] := Pi^-0.5 (1.99 - x (1 - x) (2.15 - 3.93 x + 2.7 x^2)) / ((1 + 2 x) (1 - x) ^ 1.5);

(*Correction factor for 3pb K_I,F *)
g1[x_] := 0.46 + 3.06 x + 0.84 (1 - x) ^ 5 + 0.66 x^2 (1 - x) ^ 2;
g2[x_] := -3.52 x^2;
g3[x_] := 6.17 - 28.22 x + 34.54 x^2 - 14.39 x^3 - (1 - x) ^ 1.5 - 5.88 (1 - x) ^ 5 - 2.64 x^2 (1 - x) ^ 2;
g4[x_] := -6.63 + 25.16 x - 31.04 x^2 + 14.41 x^3 + 2 (1 - x) ^ 1.5 + 5.04 (1 - x) ^ 5 + 1.98 x^2 (1 - x) ^ 2;
G[x_, y_] := g1[y] + g2[y] x + g3[y] x^2 + g4[y] x^3;
F2[x_, y_] := G[x, y] / (1 - (y)) ^ 1.5 / (1 - (x) ^ 2) ^ 0.5;

(* Stress intensity at crack tip due to a pair of point forces on the crack face *)
KIF[f_, x_, a_] := 2 f / (Pi a) ^ 0.5 F2[x / a, a / w];

(* Stress intensity at the crack tip due to remote loading in 3-point bending *)
KIP[P_, a_] := (6 / w^2) (P s / 4) (Pi a) ^ 0.5 F1[a / w]; (*P (Pi a)^0.5 F3[a/w];*)

(*Crack opening displacements from remote loading*)
ΔP[z_] :=
  2 / ee NIntegrate[KIP[Pguess, x] D[KIF[f, z, x], f], {x, z, a}, Method → {Automatic, "SymbolicProcessing" → 0},
    MaxRecursion → 0];

(*Crack closing displacements from bridging - requires nested numerical integration*)
ΔFinner[z_?NumericQ, a_?NumericQ] :=
  NIntegrate[KIF[σx[aaa], aaa, a], {aaa, c, z}, Method → {Automatic, "SymbolicProcessing" → 0},
   MaxRecursion → 0];

ΔF[z_, zz_] :=
  2 / ee NIntegrate[ΔFinner[aa, aa] D[KIF[f, z, aa], f], {aa, zz, a},
    Method → {Automatic, "SymbolicProcessing" → 0}, MaxRecursion → 0];

(*Remote load (3pb) for specified crack length and applied stress intensity*)
P[KI_, a_] := KI / (6 s / (4 w^2) (Pi a) ^ 0.5 F1[a / w]);

(*Function used in calculation of load-point displacements*)
V2[x_] := (x / (1 - x)) ^ 2 (5.58 - 19.57 x + 36.82 x^2 - 34.94 x^3 + 12.77 x^4);

Δo = Δ1;(*note the initial Δ1 guess*)

(*Initial guess for bridging zone stress distribution*)
σx0 = Interpolation[{{-20^-10, 0}, {c - 10^-10, 0}, {c, σguess}, {a, σguess}, {a + 10^-10, 0}, {w, 0}},
   InterpolationOrder → 1];
```

Estimate σ_{max} and Δ_1 Simultaneously

```
σmaxcheck = 1;(*initial value for variable that determines when to stop calculaing Δ1 and σmax estimates*)

(*Output useful information about the state of the calculation*)
Print["Crack length (a/w), σmax (MPa), Δ1 (μm), n, and Δ2 (μm)"]
Dynamic[{a/w, σmax*10^-6, Δ1*10^6, n, Δ2*10^6}]
Dynamic[ListPlot[Transpose@{Δ1list, σmaxlist}]]

While[σmaxcheck > 0, (*this loop will stop when the calculated Δ1 vs. σmax curve passes its maximum*)

  a = a0 + (Pi/2 (ee/4/KIC(Δ1))^2);
  (* set a short increment in crack growth such that the bridging zone displacements will not
   go past the guessed Δ1 value *)

  (*The adaptive mesh is very important for this calculation*)

  (*Ratios for scaling the distribution of guess points when the bridging zone changes size*)
  scale1 = (*(a-c)/(a1-a0)*)1;
  scale2 = c/a0;

  (*These values can be adjusted: higher numbers mean a denser mesh and longer calculation time*)
  xxx1 = Round[5 scale2]; (*mesh density in the short region near crack mouth*)
  xxx2 = Round[5 scale2]; (*mesh density for the majority of the non-bridged portion of the crack*)
  xxx3 = Round[5 scale2]; (*mesh density in the non-bridged region near the edge of the bridging zone*)
  xxx4 = Round[25 scale1]; (*mesh density in the short region in the bridging zone near its edge*)
  xxx5 = Round[50 scale1]; (*mesh density for the majority of the bridging zone*)
  xxx6 = Round[100 scale1]; (*mesh density near the crack tip*)

  (*Define the mesh of x-values at which the crack face displacements and stresses will be calculated*)
  cdata = Join[Array[#*0.03/xxx1&, xxx1+1, 0], Array[0.03+#*(0.96-0.03)/xxx2&, xxx2, 1],
    Array[0.96+#*(1-0.96)/xxx3&, xxx3-1, 1]];

  bridgex = Join[Array[#*0.25/xxx4&, xxx4, 1], Array[0.25+#(0.75-0.25)/xxx5&, xxx5, 1],
    Array[0.75+#(1-0.75)/xxx6&, xxx6, 1]];

  (*mesh of points for calculating stress distribution and crack-face displacements*)
  guessx = Sort[Join[cdata c, {c-10^-10, c, c+10^-10}, c+bridgex(a-c)]];

  (*Set an initial value for the error between σmax guesses*)
  σdiff = 1 000 000 000. ee; (*an arbitrarily high initial guess value that will be higher than
   the convergence criterion *)

  (*Create lists for the internal iteration process,
  where the lowest-error solution will be put into the main solution list*)
  stressevolution = {}; (*holds the stress distribution list as it converges;
  the convergent value is saved in the list defined above*)
  crackevolution = {}; (*same function, for crack shape*)
  closingevolution = {}; (*same function, for closing displacements*)
  openingevolution = {}; (*same function, for opening displacements*)
  Klist1 = {}; (*same function, for K_TR*)
  plist1 = {}; (*same function, for P*)

  σmaxguess = {}; (*same function, for σmax*)
  nguess = {}; (*same function, for n*)
  Δ1guess = {}; (*same function, for Δ1*)

  break = 0; (*initial value for a counter that allows a certain number of increases in error to occur,
  in an attempt to move past local minima towards the global minimum*)
```

```
(* Iterative loop that calculates opening profile and stresses using stress distribution
 convergence criterion *)
While[σdiff > conv,

 (*A check to make sure that the mesh of x-
  values does not force the code to attempt to make any calculations beyond the crack tip*)
 While[guessx[[Length[guessx]]] > a, guessx = Delete[guessx, -1]];

 (*Calculate the total stress intensity reduction due to the bridging zone,
 the applied stress intensity, and applied load*)
 Clear[ΔKIF, KIR, Pguess];
 ΔKIF = NIntegrate[KIF[shape[aaa] σx0[aaa], aaa, a], {aaa, c, a},
   Method → {Automatic, "SymbolicProcessing" → None}, MaxRecursion → 0];
 (*calculated stress intensity shielding due to bridging zone;
 integrals are optimized for speed and errors are reduced by multiple iterative passes*)

 (*Scale the stress distribution and the corresponding σmax guess using the known K_IR value
  for this crack length*)
 Ktrue = rcurveint[a / w] * 10^6; (*the true K_IR value for the current crack length*)
 Kratio = (Ktrue - KIC) / ΔKIF; (*this is a scaling factor for the current stress intensity
  shielding value*)

 Clear[σx];
 σx[x_] := Kratio σx0[x]; (*update the stress distribution*)

 (*recalculate values and continue using the updated stress distribution*)
 Clear[ΔKIF, KIR, Pguess];
 ΔKIF = Re[NIntegrate[KIF[ shape[aaa] σx[aaa], aaa, a], {aaa, c, a},
    Method -> {Automatic, "SymbolicProcessing" -> None}]];
 KIR = KIC + ΔKIF;
 Pguess = P[KIR, a];

 σmax =  Kratio σmax; (*update the bridging law parameter guess*)

 (*Calculate the constant value for crack face closing displacements at all points behind
  the bridging zone*)
 Clear[opening, closing, Δnet, σdist];

 (*Calculate crack face opening displacements at all mesh points*)
 opening = Array[If[guessx[[#]] ≥ a, 0, Re[ΔP[guessx[[#]]], 10^-10] &, Length[guessx]];

 (*Calculate crack face closing displacements at all mesh points*)
 (*using this loop structure prevents memory overflow*)
 counter1 = 1;
 closing = Re[Reap[
       Do[
        Sow[
         If[guessx[[counter1]] ≤ c,
          ΔF[guessx[[counter1]], c],
          ΔF[guessx[[counter1]], guessx[[counter1]]]
         ]
        ];
        ++counter1;
        , {Length[guessx]}
       ]
      ]
      [[2]]
     [[1]]
  ];

 (*Calculate net crack face displacements, preventing negative values*)
 Δnet = Array[If[opening[[#]] - closing[[#]] < 0, 0, opening[[#]] - closing[[#]]] &, Length[guessx]];

 (*Calculate crack face stresses at all mesh points using bridging law*)
 σdist =  Array[ Re[σb[Δnet[[#]]]] &, Length[guessx]];

 (*Ensure that there is no stress behind the bridging zone;
 broken ligaments are handled by the definition of σdist*)
 Do[σdist = Delete[σdist, 1]
  , {Length[Select[guessx, # < c &]]}];
 Do[PrependTo[σdist, 0]
  , {Length[Select[guessx, # < c &]]}];
```

```
 (*Make sure there are no undefined points in the functions over the entire width of the
   specimen by adding the values of each distribution at x=w*)
 AppendTo[guessx, w];
 AppendTo[σdist, 0];
 AppendTo[Δnet, 0];
 AppendTo[closing, 0];
 AppendTo[opening, 0];

 (*Interpolate over the stress distribution*)
 Clear[σinterp];
 σinterp = Interpolation[Transpose@{guessx, σdist}, InterpolationOrder → 1];

 (*Record the calculated values for this intermediate iteration to allow for examination
   of how the distribution converges to a self-consistent solution*)
 AppendTo[stressevolution, Transpose@{guessx, σdist}];
 AppendTo[crackevolution, Transpose@{guessx, Δnet}];
 AppendTo[openingevolution, Transpose@{guessx, opening}];
 AppendTo[closingevolution, Transpose@{guessx, closing}];
 AppendTo[Klist1, KIR];
 AppendTo[plist1, Pguess];

 (*prevent infinite loops*)
 If[σmax == σmaxguess[[-2]], Break[]];

 AppendTo[σmaxguess, σmax];
 AppendTo[Δlguess, Δl];

 (*check for convergence in the σmax guess*)
 If[Length[σmaxguess] > 1,
  σdiff = Abs[σmaxguess[[Length[σmaxguess]]] - σmaxguess[[Length[σmaxguess] - 1]]]
 ];

 (*update the stress distribution for the next iteration*)
 Clear[σx0];
 σx0 = σinterp;

];

(*update the check value that determines whether to continue calculating estimates for Δl and σmax*)
If[Length[σmaxlist] > 1, σmaxcheck = σmaxguess[[Length[σmaxguess]]] - σmaxlist[[Length[σmaxlist]]]
];

(*record convergent solutions for this crack length*)
AppendTo[σmaxlist, σmaxguess[[Length[σmaxguess]]]];
AppendTo[Δllist, Δlguess[[Length[Δlguess]]]];

(*increase Δl by the specified step size*)
Δl = Δl + Δlstep;
];
```

```
(*Select the best-guess point from the Δ1 vs. σmax estimate curve*)

delloop = 0;(*initial value for iterator*)
lmlist = {};(*create a list to fill with linear model fits*)

(*with each iteration, select one fewer point from the Δ1 vs. σmax curve to perform a linear regression,
then save the regression results in a list*)
Do[
 Clear[Δ1list2, σmaxlist2, lm];
 Δ1list2 = Drop[Δ1list, -delloop]; (*select the list of Δ1 values*)
 σmaxlist2 = Drop[σmaxlist, -delloop]; (*select the list of σmax values*)
 lm = LinearModelFit[Transpose@{Δ1list2, σmaxlist2}, x, x]; (*fit a line to the current set of points*)
 AppendTo[lmlist, lm];
 ++delloop;
 , {Length[Δ1list] - 2}]

rsquaredlist = Array[lmlist[[#]]["RSquared"] &, Length[lmlist]];
(*pull only the R^2 values from the list of linear models*)

(*Find the index of the first local maximum r-squared value,
which corresponds to the index of the "yield" point, counting from the right in Δ1list and σmaxlist*)
test = Array[rsquaredlist[[# + 1]] - rsquaredlist[[#]] &, Length[rsquaredlist] - 1];
index = Position[test, Select[test, # ≤ 0 &, 1][[1]]][[1, 1]];
(*Select the first value in the "test" list that has a negative value,
corresponding to the first local maximum in the list of R^2 values. This index corresponds to
 the point at which the plot of estimated Δ1 and σmax values starts to go nonlinear*)

(*Choose the final estimates for these two parameters*)
Δ1 = Δ1list[[-index]];
σmax = σmaxlist[[-index]];
Crack length (a/w), σmax (MPa), Δ1 (μm), n, and Δ2 (μm)
{0.8, 401.781, 1., 1.18989, 350}
```

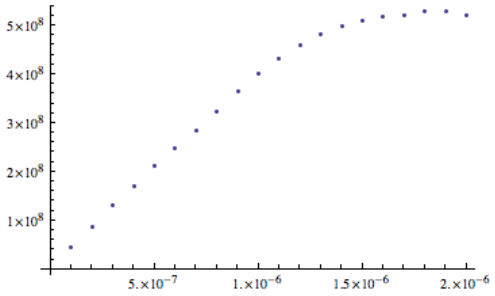

Estimate n

```
n = 100;(*high initial guesses can help n converge more quickly*)

RCurveList = {};(*create a list to hold each successive R-curve estimate as n converges*)

(*integrate the true R-curve with respect to a/w to use for scaling the n guess*)
rcurvetotal =
  NIntegrate[rcurveint[x], {x, Transpose[rcurve][[1, 1]], Transpose[rcurve][[1, Length[rcurve]]]}];

ncheck = (1 + nconv) / 2;(*initial value for the n convergence check*)

Print["Crack length (a/w),εsum, σmax(MPa),Δ1 (μm), n, and Δ2 (μm)"]
Dynamic[{a / w, εsum, σmax * 10 ^ -6, Δ1 * 10 ^ 6, n, Δ2 * 10 ^ 6}]

(*Show the convergence of the R-curves corresponding to each successive iteration in n*)
Dynamic[
 Show[
  Array[
   ListLinePlot[RCurveList[[#]], PlotStyle → Opacity[0.5, Blue]] &, Length[RCurveList] - 1
  ],
  ListLinePlot[RCurveList[[Length[RCurveList]]], PlotStyle → Opacity[1, Red]], ListPlot[rcurve],
  AxesOrigin → {0, rcurve[[1, 1]]},
  PlotRange → {{Transpose[rcurve][[1, 1]], 1},
    {0, Max[Max[Transpose[rcurve][[2]]], Max[Transpose[RCurveList[[-1]]][[2]]]]}}
 ]
]

(*Loop for varying n*)
While[ncheck > nconv,

 c = a0; (*reset the bridging zone edge to the precrack length*)
 alist = Transpose[rcurve][[1]] w;
 (*the list of crack lengths has already been defined by the true R-curve*)
 ninc = Length[alist] - 1; (*set the number of iterations to match the number of actual R-curve points*)

 (*Initial guess for bridging zone stress distribution*)
 σx = Interpolation[{{-20 ^ -10, 0}, {c - 10 ^ -10, 0}, {c, σmax}, {a, σmax}, {a + 10 ^ -10, 0}, {w, 0}},
   InterpolationOrder → 1];

 loop = 2; (*start with 2 because the first calculation occurs at the second point in the R-curve*)

 clist = {a0}; (*list for values of the end of the bridging zone calculated for each crack length*)
 Klist = {KIC}; (*list of K_IR values*)
 plist = {0}; (*list of applied loads*)
 dlist = {0}; (*list of load-point displacements*)
 error = {0}; (*list of the convergent error for the stress distribution for each crack length*)
 finalerrordist = {}; (*list of the distribution of bridging-
  stress errors along the crack face for each crack length*)
 finalstressevolution = {}; (*list of the stress distributions for each crack length*)
 finalcrackevolution = {}; (*list of the crack shapes for each crack length*)
 finalopeningevolution = {}; (*list of crack opening displacement distributions*)
 finalclosingevolution = {}; (*list of crack closing displacement distributions*)
 points = {0}; (*number of points in the mesh for each crack length*)
```

```
Do[

 a = alist[[loop]];
 (*make sure that the crack lengths used in the calculation are the same as those measured in the R-
  curve*)

 (*The following is the same as in Case 1*)

 Label["resetc"];

 If[loop == 1,
  scale1 = (a - c) / (a1 - a0);
  scale2 = c / a0;

  xxx1 = Round[5 scale2];
  xxx2 = Round[5 scale2];
  xxx3 = Round[5 scale2];
  xxx4 = Round[25 scale1];
  xxx5 = Round[50 scale1];
  xxx6 = Round[100 scale1];

  cdata = Join[Array[# * 0.03 / xxx1 &, xxx1 + 1, 0], Array[0.03 + # * (0.96 - 0.03) / xxx2 &, xxx2, 1],
    Array[0.96 + # * (1 - 0.96) / xxx3 &, xxx3 - 1, 1]];

  bridgex = Join[Array[# * 0.25 / xxx4 &, xxx4, 1], Array[0.25 + # (0.75 - 0.25) / xxx5 &, xxx5, 1],
    Array[0.75 + # (1 - 0.75) / xxx6 &, xxx6, 1]]
 ];

 guessx = Sort[Join[cdata c, {c - 10^-10, c, c + 10^-10}, c + bridgex (a - c)]];

 esum = 1 000 000 000. ee;
 elist = {esum};

 stressevolution = {};
 crackevolution = {};
 closingevolution = {};
 openingevolution = {};
 Klist1 = {};
 plist1 = {};
 error1 = {};
 errordist = {};

 break = 0;

 While[esum > conv,

  While[guessx[[Length[guessx]]] > a, guessx = Delete[guessx, -1]];

  Clear[ΔKIF, KIR, Pguess];
  ΔKIF = NIntegrate[KIF[ shape[aaa] σx[aaa], aaa, a], {aaa, c, a},
    Method → {Automatic, "SymbolicProcessing" → None}, MaxRecursion → 0];
  KIR = KIC + ΔKIF;
  Pguess = P[KIR, a];

  Clear[opening, closing, Δnet, σdist];

  opening = Array[If[guessx[[#]] ≥ a, 0, Re[ΔP[guessx[[#]]]], 10^-10] &, Length[guessx]];
```

```
counter1 = 1;
closing = Re[Reap[
      Do[
       Sow[
        If[guessx[[counter1]] ≤ c,
         ΔF[guessx[[counter1]], c],
         ΔF[guessx[[counter1]], guessx[[counter1]]]
        ]
       ];
       ++counter1;
       , {Length[guessx]}
      ]
     ]
     [[2]]
    [[1]]
 ];

Δnet = Array[If[opening[[#]] - closing[[#]] < 0, 0, opening[[#]] - closing[[#]]] &, Length[guessx]];

σdist =  Array[ Re[σb[Δnet[[#]]]] &, Length[guessx]];

Do[σdist = Delete[σdist, 1]
 , {Length[Select[guessx, # < c &]]}];
Do[PrependTo[σdist, 0]
 , {Length[Select[guessx, # < c &]]}];

AppendTo[guessx, w];
AppendTo[σdist, 0];
AppendTo[Δnet, 0];
AppendTo[closing, 0];
AppendTo[opening, 0];

Clear[σinterp];
σinterp = Interpolation[Transpose@{guessx, σdist}, InterpolationOrder → 1];

εx = σdist - Array[ Re[shape[guessx[[#]]] σx[guessx[[#]]]] &, Length[guessx]];
εsum = Sum[Abs[εx[[x]]], {x, Length[εx]}];

check = (Min[εlist] - εsum) / Min[εlist];
If[check ≤ 0, ++break];
If[break > maxbreak, Break[]];
If[break > 0, If[Abs[check] > breakcheck, Break[]]];

AppendTo[stressevolution, Transpose@{guessx, σdist}];
AppendTo[crackevolution, Transpose@{guessx, Δnet}];
AppendTo[openingevolution, Transpose@{guessx, opening}];
AppendTo[closingevolution, Transpose@{guessx, closing}];
AppendTo[Klist1, KIR];
AppendTo[plist1, Pguess];
AppendTo[error1, εsum];
AppendTo[errordist, Transpose@{guessx, εx}];
AppendTo[εlist, εsum];

Clear[σx];
σx = σinterp;

If[Min[εlist] == 0, Break[]];

];
```

```
  cguess = c;

  result = Extract[Position[error1, Min[error1]] , {1, 1}];

  Clear[crackshape, ccheck];

  crackshape = Interpolation[crackevolution[[result]], InterpolationOrder → 1];

  ccheck = If[Max[Transpose[crackevolution[[result]]][[2]]] ≥ Δ2, x /. FindRoot[crackshape[x] == Δ2, {x, a0 / 2}],
    0];

  c = Max[ccheck, a0];

  If[Abs[(c - cguess) / cguess] ≥ cconv, Goto["resetc"]];

  AppendTo[clist, c];
  AppendTo[Klist, Klist1[[result]]];
  AppendTo[plist, plist1[[result]]];
  AppendTo[error, error1[[result]]];
  AppendTo[finalstressevolution, stressevolution[[result]] ];
  AppendTo[finalcrackevolution, crackevolution[[result]] ];
  AppendTo[finalopeningevolution, openingevolution[[result]] ];
  AppendTo[finalclosingevolution, closingevolution[[result]] ];
  AppendTo[finalerrordist, errordist[[result]]];
  AppendTo[points, Length[guessx]];

  loop++;

  , {ninc}];

 (*integrate the estimated R-curve with respect to a/w*)
 Clear[rcurveEst];
 rcurveEst = Transpose@{(alist) / w, Klist / 1 000 000};
 rcurveEstInt = Interpolation[rcurveEst, InterpolationOrder → 1];
 rcurveEsttotal = NIntegrate[rcurveEstInt[x],
   {x, Transpose[rcurveEst][[1, 1]], Transpose[rcurveEst][[1, Length[rcurveEst]]]}];

 rcurveratio = rcurveEsttotal / rcurvetotal; (*set a scale factor to update the n guess*)
 n = n * rcurveratio ^ npower; (*update n, using the gain exponent npower to increase the convergence speed*)

 (*update the convergence check by calculating the fractional change in n*)
 If[Length[nlist] > 0,
  ncheck = Abs[nlist[[-1]] - n] / nlist[[-1]]
 ];

 (*record the estimates for n and for the R-curve, and repeat until n converges*)
 AppendTo[nlist, n];
 AppendTo[RCurveList, rcurveEst];

]
```

```
Crack length (a/w),εsum, σmax(MPa),Δ1 (μm), n, and Δ2 (μm)
{0.8, 65043.8, 401.781, 1., 1.18989, 350}
```